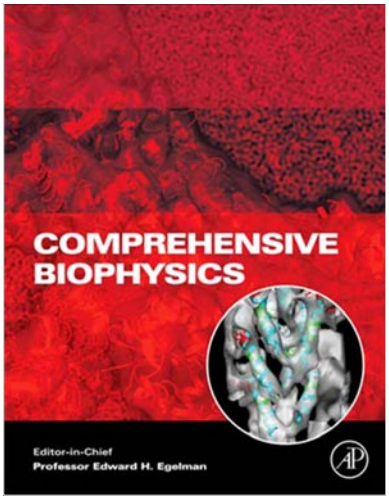

From L.S.-L. Cheung, P.S. Raman, D. Wirtz and K. Konstantopoulos, Biophysics of Selectin-Mediated Cell Adhesion. In: Edward H. Egelman, editor: Comprehensive Biophysics, Vol 7, Cell Biophysics, Denis Wirtz. Oxford: Academic Press, 2012. pp. 10-32.
ISBN: 978-0-12-374920-8

7.3 Biophysics of Selectin-Mediated Cell Adhesion

L S-L Cheung, PS Raman, D Wirtz, and K Konstantopoulos, The Johns Hopkins University, Baltimore, MD, USA

Abbreviations

2-D	two-dimensional
3-D	three-dimensional
AFM	atomic force microscope
BFP	biomembrane force probe
CR	consensus repeat
EDTA	ethylenediaminetetraacetic acid
EGF	epidermal growth factor
MFP	molecular force probe
PMN	polymorphonuclear leukocyte
RBC	red blood cell
RIC	reflectance interference contrast

Glossary

2-D binding kinetics The binding kinetics the binding kinetics between membrane-bound receptors and ligands anchored to apposing cell surfaces, whose motions are restricted to a 2-D plane.

Bell model A model proposed by Bell for describing receptor–ligand bond dissociation, wherein the bond dissociation rate increases exponentially with the applied force.

Catch bond receptor–ligand bonds whose lifetimes increase upon the application of a low external force.

Dembo model A model proposed by Dembo for describing receptor–ligand bond dissociation, wherein the bond lifetime may decrease or increase or remain the same upon application of an external force.

Micropippette aspiration assay A technique to measure the two-dimensional (2-D) kinetics of receptor–ligand interactions by characterizing the adhesion frequency as a function of contact duration between two apposing cells.

Molecular force probe A device that utilizes a flexible cantilever, which deflects in response to forces generated between the tip and the sample surface when brought together, for measuring the kinetic and micromechanical properties of receptor–ligand bonds at the single molecule level.

O-glycans The modification of serine or threonine residues on proteins by addition of a GalNAc residue, which results in an O-linked oligosaccharide or O-glycan.

PSGL-1 The P-selectin glycoprotein ligand-1 (PSGL-1; CD162) is a membrane glycoprotein that is expressed on

 doi:10.1016/B978-0-12-374920-8.00703-7

virtually all blood leukocytes, human hematopoietic progenitor cells, and to a much lesser extent on blood platelets.

Selectin A Ca^{2+}-dependent transmembrane glycoprotein present on the surface of circulating leukocytes, activated platelets, and endothelial cells at sites of inflammation/infection.

Shear threshold phenomena A counterintuitive phenomenon in which the extent of cell binding to selectins first increases and then decreases while monotonically increasing the wall shear stress.

Shear-controlled association rate An association rate model wherein the shear-induced slipping motion of a cell relative to a wall may enhance the encounter rate between membrane-bound receptors and immobilized ligands.

sLe^x The tetrasaccharide sialyl Lewis x {sLe^x; NeuAc α2,3 Gal β1,4 (Fuc α1,3) GlcNAc-R} is a terminal component of glycans attached to glycoproteins and glycolipids on most circulating leukocytes, and on some endothelial cells and tumor cells.

Slip bond receptor–ligand bonds whose lifetimes decrease with the application of an external force.

Two-pathway dissociation model A model wherein the unbinding of the selectin–ligand complex from a single bound state can be either along the catch pathway over a low-energy barrier or the slip pathway along a high-energy barrier.

7.3.1 Introduction

Cell adhesion is instrumental in diverse biological processes, including inflammation and blood-borne metastasis. In the cardiovascular system, cells are exposed constantly to hemodynamic forces generated by blood flow, including fluid shear stress. On one hand, fluid shear induces collisions among free-flowing cells as well as between free-flowing cells and the vessel wall, thereby increasing the encounter rate between membrane-bound receptors and their ligands. On the other hand, fluid shear shortens the intercellular contact duration, and exerts tensile forces tending to disrupt the receptor–ligand bonds that are responsible for cell adhesion. Cell–cell adhesive interactions, therefore, depend on the balance between the dispersive hydrodynamic forces and the adhesive forces generated by the interactions of receptor–ligand pairs.

Cell adhesion pertinent to inflammation and blood-borne metastasis is primarily regulated by two families of adhesion receptors, namely the selectins and integrins, and their respective ligands. The selectins comprise a family of three structurally related cell adhesion molecules, L-, E- and P-selectin. Each selectin has an amino terminal domain with sequence similarity to the calcium-dependent animal lectins (C-type lectins), followed by an epidermal growth factor (EGF)-like domain, variable numbers of short consensus repeat (CR) domains, a single-pass transmembrane domain, and a short cytoplasmic carboxyl terminal tail. While sharing many common elements, the tissue distribution and regulation of the three selectins are quite different, possibly reflecting their crucial involvement in a number of pathophysiological processes. L-selectin (CD62L) is constitutively expressed on the surface of almost all types of leukocytes but is rapidly shed upon cell activation with cytokines, chemokines or formyl peptides. E-selectin (CD62E) expression is induced on vascular endothelial cells, requires *de novo* mRNA and protein synthesis, and peaks 4–6 hours after activation with inflammatory stimuli *in vitro*. However, *in vivo*, E-selectin may be chronically expressed at sites of local inflammation, particularly in the blood vessels of skin during delayed hypersensitivity reactions.[1] P-selectin (CD62P) expression on both vascular endothelium and platelets is also inducible. However, P-selectin is stored preformed in the Weibel-Palade bodies of endothelial cells and alpha-granules of platelets, from which it can be rapidly mobilized (within seconds to minutes) to the plasma membrane upon cell activation.[2] Additionally, P-selectin expression on vascular endothelium may also be regulated at the transcription level. Cytokines such as interleukin-4 or oncostatin M significantly upregulate P-selectin mRNA levels in cultured human endothelial cells in a delayed and sustained fashion.[3]

Like all C-type lectins, the selectins bind to carbohydrate ligands in a calcium-dependent manner. Detailed studies involving site-directed mutagenesis, domain swapping, and antibody inhibition, have revealed that carbohydrate ligands bind to the lectin domain on a shallow region that overlaps a single calcium coordination site opposite where the EGF domain is located.[4,5] Several lines of evidence also suggest that the EGF domain and the short CR domains not only contribute to ligand specificity, but also confer unique kinetic and mechanical properties on each selectin when binding to its ligand.[6]

The selectins share the ability to recognize the tetrasaccharide sialyl Lewis x (sLe^x; NeuAc α2,3 Gal β1,4 [Fuc α1,3] GlcNAc-R) and its isomer sialyl Lewis a (sLe^a; NeuAc α2,3 Gal β1,3 [Fuc α1,4] GlcNAc-R).[4] sLe^x is a terminal component of glycans attached to glycoproteins and glycolipids on most circulating leukocytes and some endothelial cells. In contrast, sLe^a is found on some tumor cells but not on normal leukocytes. The binding affinity of selectins for isolated monovalent sLe^x and sLe^a oligosaccharides is very low, as shown in **Table 1**. Consequently, neither expression of the sLe^x nor the sLe^a groups per se correlates with the properties of endogenous selectin ligands on cellular targets. Instead, sLe^x or related structures are part of more extensive binding determinants. As pointed out by Varki,[7] distinctions must be drawn between structures that can bind to selectins under certain conditions *in vitro* and structures that actually do interact with selectins *in vivo*. To this end, a functional selectin ligand should fulfill certain criteria; it should be expressed in the right place at the right time; the ligand should bind with some selectivity and relatively high affinity; selective removal or absence of the ligand should prevent cell adhesive interactions.

High affinity ligands for P- and L-selectin have been identified. P-selectin binds to the amino terminus of the P-selectin glycoprotein ligand-1 (PSGL-1; CD162), which is expressed on virtually all blood leukocytes, human

Table 1 Three-dimensional affinity and kinetic rate constants of selectin–sLe^x interactions measured by surface plasmon resonance.

Selectin	*Ligand*	K_d *(mM)*	k_f $(M^{-1}\ s^{-1})$	k_r (s^{-1})
P-selectin	sLe^x	7.8	67 000	522
L-selectin	sLe^x	3.9	280 000	1080
E-selectin	sLe^x	0.72	230 000	164

Nicholson, M. W.; Barclay, A. N.; Singer, M. S.; Rosen, S. D.; van der Merwe, P. A. Affinity and kinetic analysis of L-selectin (CD62L) binding to glycosylation-dependent cell-adhesion molecule-1. *J. Biol. Chem.* **1998**, *273*, 763–770. Poppe, L.; Brown, G. S.; Philo, J. S.; Nikrad, P. V.; Shah. Conformation of sLe(x) tetrasaccharide, free in solution and bound to E-, P-, and L-selectin. *J. Am. Chem. Soc.* **1997**, *119*, 1727–1736.

hematopoietic progenitor cells,[8] and to a much lesser extent on blood platelets.[9] High affinity binding of PSGL-1 to P- and L-selectin requires three clustered tyrosine sulfate residues, adjacent peptide components, and fucose and sialic acid residues on an optimally positioned short core-2 O-glycan within the anionic amino-terminal region of PSGL-1.[10] Crystallographic studies reveal a patch of positive electrostatic potential on P-selectin designed to engage the tyrosine sulfate residues and increase the binding affinity.[5] L-selectin binds to PSGL-1 and glycoprotein ligands (GlyCAM-1, CD34, MadCAM-1) that contain O-linked glycans in which the sLe^x determinant is present and further substituted with a sulfate ester on the 6-hydroxyl group of the GlcNAc (NeuAc α2,3 Gal β1,4 [Fuc α1,3] $SO_3$6-GlcNAc; 6-sulfo-sLe^x) and/or Gal (NeuAc α2,3 $SO_3$6-Gal β1,4 [Fuc α1,3] GlcNAc; 6′-sulfo-sLe^x) residues. The sulfate residue on GlcNAc is required for high affinity L-selectin-dependent binding, while the contribution of Gal-6-sulfation is controversial.[11] E-selectin also binds to PSGL-1,[12] but accumulating evidence supports the concept that sialylated fucosylated glycolipids on human PMNs might be the physiologically relevant E-selectin ligands.[13–15] Recent studies also reveal that variant isoforms of CD44 (CD44v) on colon carcinoma cells possess E-, P- and L-selectin binding activity.[16–18] Interestingly, the selectin binding determinants on CD44v are sialofucosylated structures displayed on O-linked glycans, akin in nature to those on PSGL-1.

This chapter reviews both theoretical and experimental aspects of selectin-mediated cell adhesion. We first discuss the concept of two-dimensional affinity binding along with relevant mathematical models and experimental methodologies. Next, the biophysics of selectin–ligand bond rupture under applied force is reviewed, in light of observations showing that under certain conditions force can shorten or prolong the lifetime of receptor–ligand bonds, referred to as slip or catch bonds, respectively. The impact of catch-to-slip selectin–ligand bond transition on the shear-threshold phenomenon in which the number of interacting cells first increases and then decreases while monotonically increasing the shear stress is discussed. We conclude by discussing the modeling of selectin-mediated cell tethering and rolling in shear flow.

7.3.2 Two-dimensional (2-D) Receptor–Ligand Binding Kinetics

Even though several techniques have been developed to study the kinetics of receptor–ligand binding, most of them, such as radio-immunoassays and surface plasmon resonance, require at least one molecule present in solution phase, which limits their application to the measurement of three-dimensional (3-D) binding constants. However, cell adhesion is mediated by binding of membrane-bound receptors to ligands anchored to apposing cell surfaces, in which the motion of both the receptor and ligand are restricted to 2-D.[19] Not only the binding mechanism is different, but also their respective kinetic association rates have different units ($M^{-1}\ s^{-1}$ in 3-D and $\mu m^2\ s^{-1}$ in 2-D). Although 3-D kinetic rates have been extensively reported in the literature, they do not adequately describe the 2-D kinetics of selectin-mediated cell adhesion.

To quantify the 2-D receptor–ligand binding kinetics, a micropipette aspiration assay was developed by Evans and colleagues.[20–21] In this assay, a red blood cell (RBC), serving as a picoforce transducer, coated with a low density of the adhesion receptor of interest is held at a fixed position by a micropipette. Also held by a second micropipette, a polymorphonuclear leukocyte (PMN) or a ligand-decorated bead is translated to contact with the biomembrane force probe (BFP) by precision-piezo displacements for prescribed periods of time. This micropipette is then retracted from the contact position at defined pulling velocities, and the extension of the RBC induced by the molecular linkage (i.e., receptor–ligand bond) is monitored under a video-enhanced microscope. The bond rupture force is calculated by multiplying the total extension of RBC with the stiffness of the membrane transducer at the moment of the molecular linkage failure.[20,22] This technique has been utilized to determine the force-dependent 2-D dissociation rates of receptor–ligand pairs as discussed in sections 7.3.3 and 7.3.4. By precisely controlling the contact duration and quantifying the fraction of adhesive events (i.e., adhesion probability rather than adhesion strength), the micropipette aspiration assay can also evaluate the 2-D affinity per contact area, $A_c K_a^0$,[23] by using a probabilistic formulation in small systems,[24–27] as described in Section 7.3.2.2.

7.3.2.1 Mathematical Models of 2-D Receptor–Ligand Binding

The behavior of a macroscopic system is usually deterministic, since it is governed by a large population of adhesion molecules such that the spontaneous fluctuations become insignificant. Once the state of the system is known at time t, the state at any other time can be determined and no fluctuations are considered. However, when the size of system is reduced, the effect of intrinsic randomness starts to significantly affect the measurement; hence, the deterministic model may not accurately predict the behavior of the system. In this sub-

section, the kinetics of small systems and its application to micropipette aspiration assays will be discussed.[23–25]

In the micropipette experiment, the target cell or bead is typically brought into contact with the RBC, thereby forming a small overall contact zone. For such a small contact zone and relatively limited number of adhesion molecules, receptor–ligand binding occurs as a random event, and is thus non-deterministic even though all experimental conditions can be kept identical including contact area (A_c), duration (t), surface density of receptors (m_r) and ligands (m_l). Instead of using a single scalar to describe the average binding events per area, the probabilistic model is more suitable here.[25] If the probability to have n bond is defined as p_n, the state of system can be described by a vector that includes the combination of all possible states:

$$\{P_0, P_1, ..., P_n, P_{A_c m_{\min}}\} \quad [1]$$

The number of established bonds varies between 0 and $A_c m_{min}$ where $m_{min} = \min(m_r, m_l)$. For a one-step reversible kinetic system, its reaction equation is given by:

$$v_r R + v_l L \underset{k_r^0}{\overset{k_f^0}{\rightleftharpoons}} v_b B \quad [2]$$

where k_f^0 and k_r^0 represent the unstressed association and dissociation reaction rates, respectively. Equation [2] represents the general form of receptor–ligand interaction involving v_r receptors (R) binding to v_l ligands (L) to produce v_b bonds (B).

When the two cells are just brought into contact with each other, there is no bond at this instant ($t = 0$):

$$p_n(0) = \begin{cases} 1 & \text{when } n = 0 \\ 0 & \text{when } n \neq 0 \end{cases} \quad [3]$$

Once bonds start to form at $t > 0$, $p_n(t)$ increases with time t. The rates of change of these probability components are defined as:

$$\frac{dp_n}{dt} = (n+1)^{v_b} \frac{k_r^0}{A_c^{v_b-1}} p_{n+1} - \left[\left(A_c m_r - \frac{v_r}{v_b} n \right)^{v_r} \left(A_c m_l - \frac{v_l}{v_b} n \right)^{v_l} \frac{k_f^0}{A_c^{v_r+v_l-1}} + n^{v_b} \frac{k_r^0}{A_c^{v_b-1}} \right] p_n + \left[A_c m_r - \frac{v_r}{v_b}(n-1) \right]^{v_r} \left[A_c m_l - \frac{v_l}{v_b}(n-1) \right]^{v_l} \frac{k_f^0}{A_c^{v_r+v_l-1}} p_{n-1} \quad [4]$$

where the first term on the right hand side of eqn [4] represents the probability of $(n+1)$ bonds losing one bond during time t; the second and third terms represent the probability of n bonds adding one or losing one during time t, respectively; and the last term represents the probability of $(n-1)$ adding one bond during time t. Equation [4] can be simplified for two special cases.

For the first case, if the site density of one adhesion molecule is significantly higher than that of the other one, the reaction will be limited by the availability of the latter species. Therefore, $m_{max} = \max(m_r, m_l)$ is assumed to have a constant value inside the contact zone. The special case, $v_r = v_l = v_b = 1$, of this simplification has been discussed in the literature[23,24,26,27]. For this special case, the complete solution of the probability to have n bonds is in the form of binomial distribution[23]:

$$p_n(t) = \binom{A_c m_{\min}}{n} [p(t)]^n [1 - p(t)]^{A_c m_{\min} - n} \quad [5]$$

where $p(t)$ is the probability to form one bond at time t which is given by:

$$p(t) = \frac{1 - \exp\left[-(m_{\max} k_f^0 + k_r^0)t\right]}{1 + (m_{\max} k_f^0 / k_r^0)^{-1}} \quad [6]$$

For the second case, we assume the formation of a small number of receptor–ligand bonds, which will have no significant effect on the availability of unbound receptors and ligands inside the contact area. The master equation can thus be simplified by neglecting n and n–1 terms in the $[A_c m_j - (v_j/v_b)n]$ and $[A_c m_j - (v_j/v_b)(n-1)]$ (subscript $j = r$ or l)[23]:

$$\frac{dp_n}{dt} = (n+1)^{v_b} \frac{k_r^0}{A_c^{v_b-1}} p_{n+1} - \left[(A_c m_r)^{v_r} (A_c m_l)^{v_l} \frac{k_f^0}{A_c^{v_r+v_l-1}} + n^{v_b} \frac{k_r^0}{A_c^{v_b-1}} \right] p_n + (A_c m_r)^{v_r} (A_c m_l)^{v_l} \frac{k_f^0}{A_c^{v_r+v_l-1}} p_{n-1} \quad [7]$$

For the special case of $v_b = 1$, the master equation is further simplified,[28] as follows:

$$\frac{dp_n}{dt} = (n+1) k_r^0 p_{n+1} - \left(A_c m_r^{v_r} m_l^{v_l} k_f^0 + n^{v_b} k_r^0 \right) p_n + A_c m_r^{v_r} m_l^{v_l} k_f^0 p_{n-1} \quad [8]$$

The complete solution of eqn [8] is of the form of the Poisson distribution:[23,29]

$$P_n(t) = \frac{\langle n \rangle^n}{n!} \exp(-\langle n \rangle) \quad [9]$$

where $\langle n \rangle$ is the average number of bonds at time t given by:

$$\langle n \rangle = A_c m_r^{v_r} m_l^{v_l} K_a^0 \left[1 - \exp\left(-k_r^0 t\right) \right] \quad [10]$$

Both approximations provided by eqns [5] and [9] have been utilized to study the 2-D kinetics of receptor–ligand bond formation.[23,26,29,30] These approximations will deviate significantly from the exact solution when the number of available receptors and ligands are similar (i.e., $m_{max} \approx m_{min}$). The comparison between the two approximations and the exact solution against the m_{max} to m_{min} ratio has been discussed in the literature.[23] The analysis reveals that when $A_c m_{min} / \langle n \rangle > 10$, the Poisson distribution given by eqn [9] is in excellent agreement with the exact solution. In contrast, the binominal distribution, eqn [5], provides reasonable agreement with the exact solution when $m_{max}/m_{min} > 100$. Taken together, the Poisson approximation is preferable to model the 2-D receptor–ligand binding in small systems.[23]

Even though the specific case, which assumes $\nu_r = \nu_l = \nu_b = 1$, successfully fits to many experimental results,[31–34] the actual order of the reaction kinetics has to be determined. This can be obtained by fitting the Poisson equation with experimental results. Since the orders of association (ν_r and ν_l) are lumped into one value, which can be treated as a fitting parameter, the order of dissociation ν_b can be independently obtained from the fitting analysis.[23]

7.3.2.2 Estimation of Kinetic Rate Constants from Micropipette Aspiration Assays

In most chemical reactions, the concentration of the product is proportional to the reaction time until the system reaches equilibrium. Similar reaction characteristics have been observed in receptor–ligand mediated cell adhesion to a surface.[23] An example plot showing the dependence of adhesion probability on the contact duration for different site densities of membrane-bound receptors and immobilized ligands is presented in **Figure 1**. The non-specific binding P_{non} can be subtracted from the total adhesion probability P_t by the following equation:[23,35,36]

$$P_a = \frac{P_t - P_{non}}{1 - P_{non}} \qquad [11]$$

where P_a is probability of specific adhesion. For a first order binding kinetics ($\nu_r = \nu_l = \nu_b = 1$), and taking into consideration that the adhesion event is defined as having $n \geq 1$ bonds, the equation of Poisson approximation becomes:

$$\begin{aligned} P_a(t) &= 1 - P_0(t) \\ &= 1 - \exp\left\{-A_c m_r m_l K_a^0 \left[1 - \exp\left(-k_r^0 t\right)\right]\right\} \end{aligned} \qquad [12]$$

The 2-D binding affinity K_a^0 and the unstressed dissociation rate k_r^0 can be obtained by a simple graphic representation method, as shown in **Figure 1**. By setting $t \to \infty$ in eqn [12], the steady-state solution $P_{a,ss}$, which represents the maximum adhesion probability for a given set of conditions, is provided by:

$$P_{a,ss} = 1 - \exp\left(-A_c m_r m_l K_a^0\right) \qquad [13]$$

Hence, the 2-D affinity constant $A_c K_a^0$ can be estimated directly from the experiment data for a prescribed set of receptor and ligand site densities. Mathematical manipulations[23] reveal that the unstressed dissociation rate k_r^0 can be expressed by

$$k_r^0 \approx \frac{0.5}{t_{50}} \qquad [14]$$

Thus, the unstressed dissociation rate can be estimated from the time t_{50}, which represents the required time for $P_a(t)$ to achieve 50% of its steady-state value $P_{a,ss}$ (**Figure 1**).

For the very initial state ($k_r^0 t \to 0$), the initial-state solution $P_{a,int}$ can be obtained by using Taylor series expansion of the exponential functions in eqn [12] and dropping the $O\left(k_r^0 t\right)^2$ term:

$$\begin{aligned} P_{a,\mathrm{int}}(t) = 1 \\ - \exp\left\{-A_c m_r m_l K_a^0 \left[1 - \left(1 - k_r^0 t + O(k_r^0 t)^2\right)\right]\right\} \end{aligned} \qquad [15]$$

$$P_{a,\mathrm{int}}(t) = 1 - \left[1 - A_c m_r m_l K_a^0 k_r^0 t + O(k_r^0 t)^2\right] \qquad [16]$$

$$P_{a,\mathrm{int}}(t) = A_c m_r m_l k_f^0 t \qquad [17]$$

Taking the time derivative of eqn [17], the initial slope of adhesion probability can be expressed by:

$$\frac{dP_{a,\mathrm{int}}}{dt} = A_c m_r m_l k_f^0 \qquad [18]$$

According to eqn [18], the unstressed association rate k_f^0 can be estimated from the slope of the initial data points. Since the unstressed dissociation rate k_r^0 of selectin molecules is considerably large (ranging from 1 to 10 s^{-1}), dropping of $O\left(k_r^0 t\right)^2$ becomes unrealistic, and as such this method for estimating k_f^0 is inaccurate. Although no direct estimation of k_f^0 is available, an alternative expression of association $A_c k_f^0$ can be obtained by multiplying 2-D binding affinity $A_c K_a^0$ with unstressed dissociation rate k_r^0.

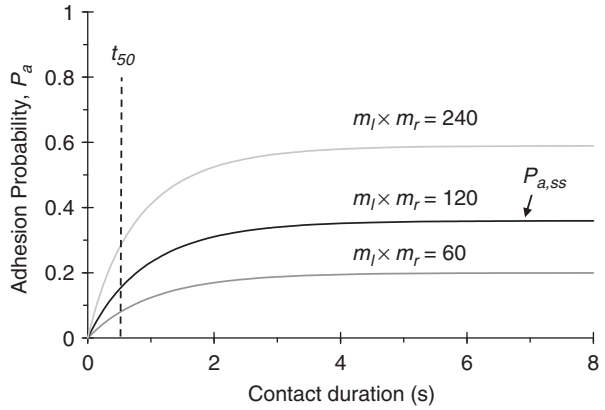

Figure 1 An example plot illustrating the adhesion probability as a function of the contact duration time for different site densities of receptors and ligands ($m_r \times m_l$). The 2-D binding affinity $A_c K_a^0$ can be estimated from eqn [13] and the steady-state data point $P_{a,ss}$. The unstressed dissociation rate k_r^0 can be determined by applying the half-time t_{50} to the eqn [14].

7.3.2.3 Effects of Cell Mechanics, Surface Microtopology, Molecular Orientation and Length on 2-D Selectin–Ligand Binding as Assessed by Micropipette Aspiration Assays

To evaluate the effects of cell stiffness and surface microtopology on the 2-D selectin–ligand binding kinetics, three types of molecule-bearing carriers have been employed in micropipette aspiration assays:[35,36] a human RBC with a deformable and relatively smooth surface; a human HL-60 cell with a less deformable and rough surface; and a polystyrene bead with a stiff and smooth surface. Comparison of systems I to III suggests that stiffening the carrier significantly reduces the 2-D binding affinity whereas it has no effect on the unstressed dissociation rate

Table 2 Summary of the 2-D unstressed dissociation rate k_r^0 and binding affinity $A_cK_a^0$ between P-selectin and PSGL-1 coated on different carriers.

System	*P-selectin bearing carrier*	*PSGL-1-bearing carrier*	k_r^0 (s^{-1})	$A_cK_a^0 \times 10^3$ (μm^4)
I	RBC	RBC	0.6 ± 0.1	22.5 ± 7.9
II	RBC	Bead	0.7 ± 0.1	4.6 ± 1.8
III	Bead	Bead	0.8 ± 0.1	0.055 ± 0.001
IV	RBC	HL-60	0.9 ± 0.1	3.7 ± 0.2

Wu, L.; Xiao, B.; Jia, X.; Zhang, Y.; Lu, S.; Chen, J.; Long, M. Impact of carrier stiffness and microtopology on two-dimensional kinetics of P-selectin and P-selectin glycoprotein ligand-1 (PSGL-1) interactions. *J. Biol. Chem.* **2007**, *282*(13), 9846–9854.

Table 3 2-D Selectin–ligand binding affinity $A_cK_a^0$ and unstressed dissociation rate k_r^0 estimated for different lengths and molecular orientations of P- or E-selectin-coated RBCs and PSGL-1-expressing on HL-60.

System	*Molecule*	*Length*	*Orientation*	k_r^0 (s^{-1})	$A_cK_a^0 \times 10^3$ (μm^4)
I	sPs	Long	Uniform	0.9 ± 0.1	3.71 ± 0.16
II	sPs	Long	Random	1.1 ± 0.1	1.18 ± 0.03
III	PLE	Short	Uniform	1.1 ± 0.1	1.63 ± 0.04
IV	sEs		Uniform	0.9 ± 0.5	0.18 ± 0.03
V	sEs		Random	0.9 ± 0.1	0.03 ± 0.001

Huang, J.; Chen, J.; Chesla, S. E.; Yago, T.; Mehta, P.; McEver, R. P.; Zhu, C.; Long, M. Quantifying the effects of molecular orientation and length on two-dimensional receptor–ligand binding kinetics. *J. Biol. Chem.* **2004**, *279*(43), 44915–44923.

(Table 2).[36] The authors[36] hypothesized that stiffening the carrier reduces the accessibility of a receptor to a ligand on an apposing surface, thereby limiting bond formation. However, the marked decrease of the 2-D binding affinity observed using the stiff vs. the deformable molecule-bearing carrier might be attributed at least partly to the smaller contact area A_c. On the other hand, the receptor–ligand bond dissociation depends on the conformation of the established complex. According to Wu et al. (2007), once a bond is successfully formed, the mechanical properties of the carrier have no effect on the probability of dissociation, as shown in Table 2.

Comparison of systems I to IV reveals that surface microtopology also affects the 2-D receptor–ligand binding kinetics. Roughing the carrier surface reduces the effective contact area A_c, which in turn decreases the effective binding affinity.[36] Interestingly, the values of the 2-D selectin–ligand binding affinity are similar for systems II and IV, suggesting that softening the carrier and roughing the surface simultaneously may have opposing effects on affinity.

By controlling the number of CR domains, P-selectin molecules of different lengths were engineered. Under static (no-flow) conditions, PSGL-1-expressing PMNs attach to both native P-selectin and P-selectin constructs containing as few as two CR domains with similar efficiency.[6] In contrast, P-selectin constructs containing only two or three CR domains failed to support PMN binding under physiological flow conditions.[6] Micropipette aspiration assays were performed to determine the impact of CR domains on the 2-D selectin–ligand binding kinetics using two types of soluble P-selectin: sPs consisting of Lec-EGF domains plus nine CR but no transmembrane and cytoplasmic domains, and PLE consisting of only the Lec-EGF domains with an added C-terminal epitope. As shown by,[35] the 2-D affinity $A_cK_a^0$ of the long sPs molecule is ~2-fold larger than that of short PLE molecules (Table 3). However, the values of the unstressed dissociation rate k_r^0 are similar in the two systems (Table 3). These findings suggest that the absence of PMN binding to immobilized P-selectin constructs bearing two or less CR domains[6] is attributed to the poor accessibility of the short molecule to the ligand-coated surface. Once P-selectin–ligand bonds form, their dissociation is not affected by the length of the molecules.

Micropipette aspiration assays were also performed to evaluate the effects of molecular orientation on 2-D selectin–ligand binding kinetics using sPs or soluble E-selectin (sEs) either adsorbed randomly on the RBC surface or coupled uniformly to non-blocking anti-selectin monoclonal antibodies-bearing RBCs. As shown by,[35] the 2-D binding affinity $A_cK_a^0$ of uniformly oriented P- or E-selectin is markedly higher than that of randomly absorbed P- or E-selectin. However, the unstressed dissociation rates k_r^0 are nearly identical. Taken altogether, cell deformability, molecular orientation, and length of selectin molecules enhance the 2-D binding affinity without affecting the unstressed dissociation rate.

7.3.3 Selectin–Ligand Dissociation: Slip Bond Kinetic Parameters

The kinetic and micromechanical properties of selectin–ligand bonds were initially estimated *in vitro* by quantifying leukocyte tethering lifetime in flow chamber assays.[13,37–39] However, these assays may not effectively differentiate avidity from affinity of a single receptor–ligand pair, and most importantly, rely on broad assumptions to estimate the forces exerted on the bonds. These issues can be addressed by the use of a BFP and a molecular force probe (MFP), which enable us to study receptor–ligand binding kinetics at the single molecule scale and determine rupture forces with pN resolution.[12,40–46] In this section, we review the experimental methodologies and

mathematical models to study the biophysical properties of the different selectin–ligand pairs at the single molecule level.

7.3.3.1 Single-molecule Force Spectroscopy

Two types of ultrasensitive probes are utilized in single-molecule force spectroscopy studies: BFP where force is sensed by the displacement of a glass microsphere immobilized on a pressurized membrane capsule (i.e., RBC),[41,42] and MFP where force is sensed by the deflection of a thin cantilever.[12,40,44–46] Both techniques allow detection of a wide force spectrum ranging from 5 pN to >1 nN,[48–56] which covers the typical biological forces from the molecular to the cellular level as tabulated in **Table 4**.

The BFP was developed based on the micropipette aspiration technique, which determines the rupture force by the deformation of membrane capsule (see section 7.3.2). Evans and colleagues[22] improved the micropipette aspiration assay by biochemically coupling a 2–3 μm diameter microsphere onto the RBC. The soft membrane capsule (RBC) becomes the force transducer, and its membrane tension is adjusted by the micropipette suction pressure. The implementation of reflectance interference contrast (RIC) microscopy enhances the resolution of detection of movement of the BFP tips to the nm level.[22] The difference between micropipette translation and BFP tip displacement is multiplied by the force constant to obtain the rupture force. The loading rate can be calculated by the product of membrane transducer force constant and the speed of separation.

The MFP has the architecture of the atomic force microscope (AFM). The MFP utilizes a flexible cantilever, which deflects in response to forces generated between the tip and the sample surface when brought together hundreds of times. Deflections are detected by a laser incident on the tip of the cantilever and, using the bending constant of the cantilever, transformed into time-dependent forces. In this sub-section, we focus on the review of the MFP technique, since detailed discussions of BFP can be found elsewhere.[22,43,47]

MFP experiments were initially performed by repeatedly bringing the receptor-functionalized cantilever into contact with a counter-receptor immobilized onto a glass slide.[53] Subsequent MFP experiments were performed using a receptor-functionalized cantilever and a cell immobilized onto a culture dish (**Figure 2**).[12,54] Cells can also be immobilized on a cantilever tip, thereby enabling us to probe receptor–ligand interactions between apposing intact cells.[55] Probing intact cells rather than recombinant proteins ensures that the natural orientation of cell receptors on the cell surface and the post-translational modifications of these receptors (e.g., glycosylation) are preserved. Moreover, using intact cells rather than recombinant proteins ensures that transmembrane receptors can still interact with the cytoskeleton via interactions mediated by cytoplasmic proteins binding the cytoplasmic domain of the receptors, while recombinant proteins tethered to reconstituted phospholipid membranes cannot. However, when probing cell–cell interactions, the non-linear mechanical response of cell deformation may complicate the measurement results.[48,56]

Receptor–ligand binding depends, among other parameters, on the contact duration between the receptor and the ligand, and the force applied by the receptor-functionalized cantilever to the immobilized cell during contact (**Figure 2(a)**). To limit the number of bonds formed during receptor–ligand contacts, the contact duration and the impinging force can be reduced. Small impinging forces and short times of interaction diminish the number of intercellular bonds. Engagement of single bonds as opposed to multiple bonds is promoted by targeting a percentage of successful receptor–ligand binding interactions of 10–35%. As discussed in section 7.3.2.1, the probability of formation of receptor–ligand bonds follows Poisson statistics. When only 30% of receptor–ligand contacts lead to molecular bonds on the force-distance curves, then >80% of the successful binding events involve only one bond, 15% involve two bonds and <3% involve three bonds. The unbinding of single receptor–ligand pairs is also revealed by the emergence of predominantly single rather than multiple steps in the force-time traces (**Figure 2(b)**). Under these conditions, rupture force histograms, representing the most probable rupture force at a given reproach velocity, develop a single peak as opposed to regularly spaced force distributions, which would be indicative of the unbinding of oligomeric adhesions.[57]

Control experiments are performed to demonstrate the specificity of receptor–ligand binding. For instance, addition of ethylenediaminetetraacetic acid (EDTA) to the tissue culture dish consistently abrogated binding (**Figure 2(b)**), a finding which is in agreement with the calcium dependence of selectin–ligand binding. Alternatively, incubating the selectin-coated cantilever with a function-blocking anti-selectin mAb or the neutrophils with an anti-PSGL-1 mAb reduces the frequency of binding events to basal levels.

A wide variety of receptor–ligand pairs, such as E-cadherin or N-cadherin homotypic binding, selectin–ligand or integrin–vascular cell adhesion-1 binding, have been studied by BFP and/or MFP.[12,41,42,44,54,55,58,59] Before summarizing the force-spectroscopy data on selectin–ligand binding interactions at the single molecule level, we will review the kinetic models of receptor–ligand bond dissociation.

Table 4 Characteristic force scales of common cellular and molecular processes

Biological processes	*Force scale*	*References*
Cellular contraction	~0.1–1 mN	121
Protein unfolding	~100–200 pN	122–124
Receptor-ligand interaction	~50–250 pN	(Hanley et al., 2004; 12,125)
Cytoskeletal motor protein	~2–10 pN	126

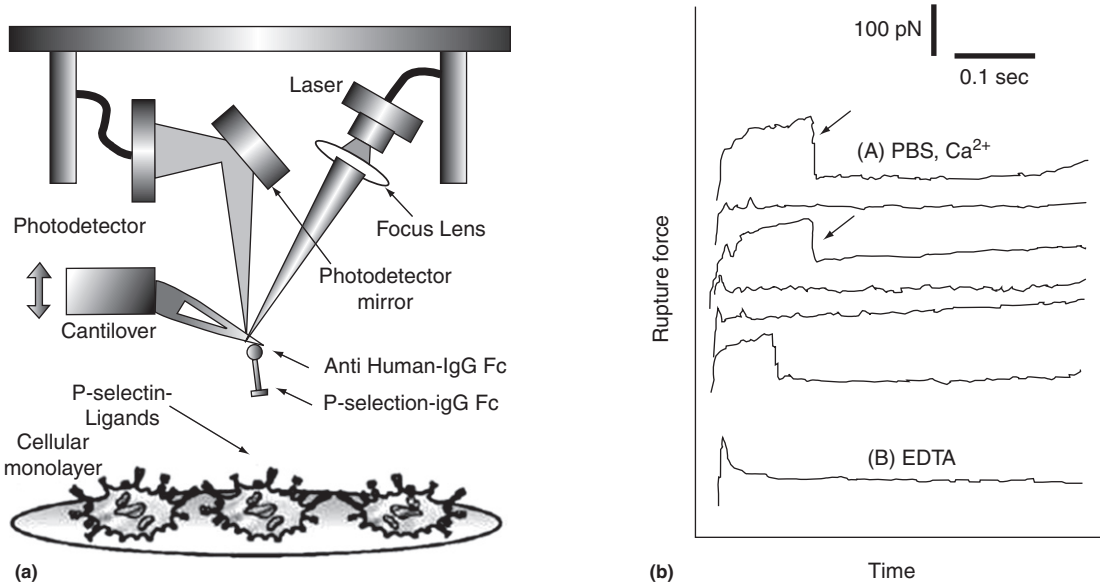

Figure 2 (a) MFP schematic indicating the use of intact cells to measure *in situ* cellular adhesion forces. P-selectin-Ig chimera was captured in the proper orientation with an anti-human IgG/Fc antibody adsorbed on the cantilever tip. The cantilever was positioned directly above a cell and was allowed to approach until it touched and slightly deformed the cell membrane before reproaching at a prescribed velocity. This approach/reproach cycle was repeated hundreds of times to obtain a statistically significant value for the P-selectin–ligand rupture force. Adapted with permission from Hanley, W.; McCarty, O.; Jadhav, S.; Tseng, Y.; Wirtz, D.; Konstantopoulos, K. Single molecule characterization of P-selectin/ligand binding. *J. Biol. Chem.* **2003**, *278*(12), 10556–10561. Copyright by American Society for Biochemistry and Molecular Biology. (b) Force versus time traces for E-selectin binding to PMNs in the absence (curve A) and presence (curve B) of EDTA. Experimental conditions, including selectin concentration on the cantilever, contact force and dwell time, were optimized for P-, E- and L-selectin experiments to result in ~30% binding events (30 adhesion events per 100 contacts). The arrows indicate rupture events with magnitudes of about 100 pN taken from an experiment with a reproach velocity of 15 μm/s. The presence of EDTA was consistently found to eliminate receptor–ligand binding. The linear increase in slope just before each rupture event is indicative of the loading rate exerted on the receptor–ligand bond. Adapted with permission from Hanley, W. D.; Wirtz, D.; Konstantopoulos, K. Distinct kinetic and mechanical properties govern selectin-leukocyte interactions. *J. Cell. Sci.*, **2004**, *117*(Pt 12), 2503–2511. Copyright by Company of Biologists.

7.3.3.2 Mathematical Description of Slip-Bond Dissociation

When a receptor and a ligand are in close proximity to each other, the bond formation can be described by a reversible bimolecular reaction with two discrete steps: receptor–ligand encounter and reaction. This conceptual design[60] is expressed by:

$$R + L \underset{d_-}{\overset{d_+}{\rightleftharpoons}} RL \underset{r_-}{\overset{r_+}{\rightleftharpoons}} \text{Bond} \qquad [19]$$

where R is a free selectin molecule, L is a free ligand molecule, d_+ and d_- are the rates of formation and dissociation of the encounter complex RL, r_+ and r_- are the forward and reverse rate for the bond formation. In most cases, the concentration of RL complex is significantly lower than that of free receptor R and free ligand L. Therefore, eqn [19] can be simplified by assuming each bond is formed directly from the pair of free molecules.[60] The overall binding process is thus represented by:

$$R + L \underset{k_r}{\overset{k_f}{\rightleftharpoons}} \text{Bond} \qquad [20]$$

where k_f and k_r are the association and dissociation rates of the bond resulting from a free receptor and a free ligand pair. In 1978, Bell proposed the force dependence of receptor–ligand bond dissociation, which is given by:

$$k_r(f) = k_r^0 \exp\left[\frac{x_\beta f}{k_B T}\right] \qquad [21]$$

where k_r^0 is the unstressed dissociation rate, x_β is reactive compliance, f is the rupture force acting on the bond, k_BT is the Boltzmann constant multiplied by the temperature (or thermal energy). The bond dissociation rate k_r, which is related to bond lifetime t_b by $t_b = 1/k_r$, exponentially increases with the applied force as shown in **Figure 3(a)**. In the literature, k_r is also given in the following form:[43,61]

$$k_r(f) = k_r^0 \exp\left[\frac{f}{f_\beta}\right] \qquad [22]$$

The new parameter $f_\beta = k_BT/x_\beta$ has units of force, and can be considered as the characteristic force scale at which the dissociation rate changes 2.7-fold. Equations [21] and [22] are commonly used to model slip-bond dissociation under force.

In a BFP or MFP experiment, it is essentially impossible to apply a force instantaneously; thus, there is always a finite loading rate r_f. Evans and colleagues[62] proposed a model to estimate dissociation parameters when a bond is ruptured by a finite loading rate. The probability of a single bond rupture in

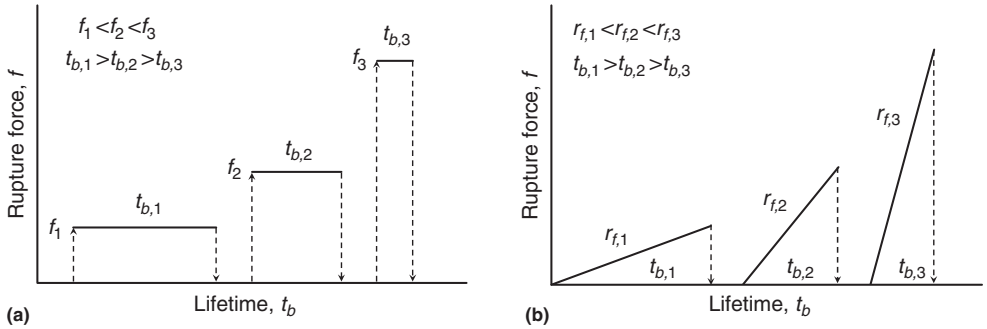

Figure 3 The bond lifetimes under (a) constant rupture forces and (b) a linear ramping of rupture force, $df/dt = r_f$. Modified with permission from Evans, E. A.; Calderwood, D. A. Forces and bond dynamics in cell adhesion. Science, **2007**, *316*(5828), 1148–1153. Copyright by AAAS.

the time interval $(t, t + dt)$ as a function of force is given by:[62]

$$p(t,f) = k_r(f)\exp\left\{-\int_0^t k_r[f(t')]dt'\right\} \quad [23]$$

where the exponential term represents the probability of bond survival up to time t, whereas the $k_r(f)$ term represents the probability of bond rupture in the next short time interval dt. The peak value of this probability distribution can be obtained by taking the derivative of eqn [23] with respect to f. By setting $\partial p/\partial f = 0$ and using the linear ramp of force, $f(t) = r_f \cdot t$, the dissociation rate at the critical rupture force $\langle f_b \rangle$ is given by:

$$k_r(\langle f_b \rangle) = r_f \frac{\partial}{\partial f}[\ln k_r(f)]_{f=\langle f_b \rangle} \quad [24]$$

Substituting the Bell model given by eqn [21] into eqn [24], eqn [25] is obtained:

$$\langle f_b \rangle = \frac{k_B T}{x_\beta}\ln\left(\frac{x_\beta}{k_r^0 k_B T}\right) + \frac{k_B T}{x_\beta}\ln(r_f) \quad [25]$$

Equation [24] suggests that the bond dissociation rate increases with the loading rate r_f as shown in **Figure 3(b)**. Interestingly, according to eqn [25], the bond rupture force also increases with the loading rate (**Figure 3(b)**). By plotting the rupture force $\langle f_b \rangle$ against the logarithm of loading rate $\ln(r_f)$, the Bell model parameters, k_r^0 and x_β, can be estimated from the slope and intercept of experimental data in the linear region by using the following equations:[12,61,63]

$$\text{slope}: \frac{k_B T}{x_\beta};\ \text{intercept}: \frac{k_B T}{x_\beta}\ln\left(\frac{x_\beta}{k_r^0 k_B T}\right) \quad [26]$$

Alternatively, k_r^0 and x_β can also be estimated by a non-linear least-square fit of eqn [27] to the experimental data over the entire range of loading rates[44,62,63]:

$$\langle f_b \rangle = \frac{k_b T}{x_\beta}\exp\left(\frac{k_r^0 k_b T}{x_\beta r_f}\right)\int_1^\infty \frac{\exp\left(\frac{-k_r^0 k_b T}{x_\beta r_f}t\right)}{t}dt \quad [27]$$

The accuracy of the Bell model parameters can be validated by Monte Carlo simulations of receptor–ligand bond rupture under constant loading rates.[12,44] In brief, given a k_r^0 and x_β in each simulation, the rupture force ($F_{rup} = r_f \times n\Delta t$) at a prescribed loading rate can be calculated for which the probability of bond rupture, P_{rup}, is greater than P_{ran}, a random number between 0 and 1:

$$P_{rup} = 1 - \exp\left[-k_r^0 \exp\left(\frac{x_\beta r_f n\Delta t}{k_b T}\right)\Delta t\right] \quad [28]$$

where $n = 1, 2, 3, \ldots$, Δt is the interval and $n\Delta t$ is the time step.

7.3.3.3 Kinetic and Micromechanical Properties of Selectin–Ligand Bonds

Using single-molecule force-spectroscopy, the dissociation of E-, P- and L-selectin from PSGL-1 presented on the neutrophil surface has been studied over a physiological range of loading rates.[12,41,44–46] In **Figure 4**, the mean rupture forces are plotted as a function of the loading rate for all three selectins.[12] The Bell model parameters, k_r^0 and x_β, were extracted by fitting eqn [26] or [27] to the experimental data shown in **Figure 4**. The trends of these parameters are summarized below:

$$\text{unstressed dissociation rate, } k_r^0: \quad \text{P} < \text{E} < \text{L}$$

$$\text{reactive compliance, } x_\beta: \quad \text{E} < \text{P} < \text{L}$$

This analysis reveals that L-selectin-PSGL-1 bonds have an intrinsically higher off-rate and a higher reactive compliance, which reflects the susceptibility of bond rupture under force. It is also clear from the force spectra that the tensile strength of an L-selectin-PSGL-1 bond is apparently lower than that of P- or E-selectin binding to PSGL-1 (**Figure 4**). Taken together, these data may help explain the faster rolling of neutrophils over L-selectin relative to E- or P-selectin in flow-based adhesion assays.[37,38]

E-selectin-PSGL-1 binding has a slightly higher k_r^0 but a lower reactive compliance x_β compared to P-selectin-PSGL-1. A higher unstressed dissociation rate suggests that E-selectin-PSGL-1 bonds have a shorter lifetime in the absence of force, however a lower reactive compliance suggest that E-selectin-PSGL-1 bonds are more resistant to rupture in the presence of force, which becomes clear at high loading rates (**Figure 4**). Because dynamic leukocyte adhesion assays are performed in

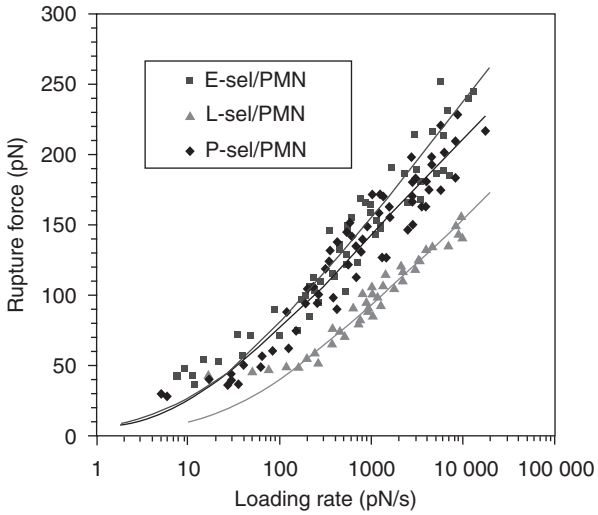

Figure 4 Rupture force plotted against the natural logarithm of loading rate for E-, P- and L-selectin binding to PSGL-1. The superimposed solid lines indicate the nonlinear least-squares fit of eqn [27] over the entire range of experimental loading rates. Adapted with permission from Hanley, W. D.; Wirtz, D.; Konstantopoulos, K. Distinct kinetic and mechanical properties govern selectin-leukocyte interactions. *J. Cell. Sci.*, **2004**, *117*(Pt 12), 2503–2511. Copyright by Company of Biologists.

the presence of hydrodynamic shear, the lower reactive compliance and additional tensile strength of E-selectin-PSGL-1 bonds might allow neutrophils to roll more slowly on E-selectin relative to P-selectin. Nevertheless, the differences in the rolling velocities of neutrophils on E- versus P-selectin-coated substrates are subtle relative to those on L-selectin.

The unstressed dissociation rates obtained by single-molecule force spectroscopy[44,47,53] typically yield lower values than those reported by flow-chamber experiments.[37–39,64] Moreover, the reactive compliance values are higher in force-spectroscopy than in flow-chamber experiments. Because multivalent binding is expected to decrease the reactive compliance, we speculate that force-spectroscopy experiments are more likely to isolate single-molecule interactions than flow chamber assays.[12] Despite the low site densities of adhesion molecules in flow chamber experiments, cell flattening during tethering and the resulting increase in the contact surface area increases the probability of mutiple selectin–ligand bonds forming, particularly at higher shear stresses.[41]

7.3.3.4 Limitations of the Bell Model Selectin–Ligand Dissociation at Low Forces

The Bell model was proposed to describe receptor–ligand bonds, referred to as slip bonds, whose lifetimes decrease with the application of an external force, because force reduces the energy barrier between the bound and free states. Ten years later, Dembo proposed an alternative model in which the dissociation rate increases exponentially with the square of applied force.[65] As a theoretical possibility, Dembo suggested that the bond lifetime, which is the inverse of dissociation rate, may also increase with the applied force or remain the same; these bonds were termed as catch and ideal bonds, respectively.

Catch-to-slip bond transition exhibited by selectin–ligand bonds under progressively increasing forces has been demonstrated experimentally.[45,46,66] This catch-to-slip bond transition is thought to be primarily responsible for the shear threshold phenomenon observed in flow-based adhesion assays where the extent of neutrophil binding to selectins first increases and then decreases while monotonically increasing the wall shear stress.[67,68] Hence, the Bell (slip-bond) model is only suitable for selectin–ligand dissociation under relatively high applied forces.

7.3.4 Selectin–Ligand Bonds Exhibit Catch Bond Behavior

Catch binding is a fascinating and counterintuitive phenomenon in which the receptor–ligand bond resists breaking and becomes stronger upon application of a low external force. At least three distinct receptor–ligand pairs have been identified to exhibit catch bond behavior: selectin–ligand,[45,46,66] glycoprotein Ib-von Willebrand factor[69] and the bacterial adhesion protein FimH-mannose.[70] This seemingly paradoxical phenomenon at the nanoscale level translates into a complex behavior witnessed at the cellular level, such as the shear-enhanced cell adhesion. In this section, we will review the catch-bond phenomenon in selectin molecules by using physical modeling and experimental evidence reported in literature.

7.3.4.1 Hookean Model of Receptor–Ligand Bond Dissociation

Dembo and his coworkers were the first to describe the catch bond behavior by assuming that the bound state and the transition state are Hookean springs with specific elastic constants and resting lengths. Originally derived from the transition state theory, the system was assumed to be close to thermodynamic equilibrium. If the bound state and the transition state springs have the same elastic constant but the transition state spring has a longer resting length than the bound state spring, the dissociation rate k_r can be expressed as an exponential function of the applied force f:[65]

$$k_r = k_r^0 \exp\left(\frac{(\delta\lambda)f}{k_B T}\right) \qquad [29]$$

where k_r is the dissociation rate in the presence of applied force f, k_r^0 is the unstressed dissociation rate, $\delta\lambda$ is the difference between the resting lengths of the transition-state and the bound-state spring ($\delta\lambda > 0$). If both springs have the same resting lengths but the transition state spring is softer, the dissociation rate increases exponentially as the square of the force:[65]

$$k_r = k_r^0 \exp\left(-\frac{(\delta k)f^2}{2k^2 k_B T}\right) \qquad [30]$$

where k is the elastic constant of the bound-state and δk is the difference between the elastic constants of the transition-state and the bound-state ($\delta k < 0$). To explain the distinctions between

slip and catch bonds, the possibilities of the transition state spring having a smaller resting length than the bound state spring ($\delta\lambda < 0$) or the transition state spring being stiffer than the bound state spring ($\delta k > 0$) were considered. This would result in the dissociation rate being an exponentially decreasing function of the force or the square of force. The elastic constant and the resting lengths of the two states can be allowed to be different at the same time, for which the full model can be expressed as:[65]

$$k_r(f) = k_r^0 \exp\left\{\frac{(\delta\lambda)f - \frac{\delta k}{2k^2}f^2}{k_B T}\right\} \quad [31]$$

In the above equation, the dissociation rate depends exponentially on a quadratic function of force. This is the simplest three-parameter model proposed for explaining catch bonds. It was thought that the application of external force on the catch bond decreases its failure rate at low forces, but this scenario switches to the traditional slip binding at higher forces where the applied force increases the failure rate. A simple physical model to explain the catch bond behavior is that of a child's toy called the finger-prison: the harder you try to pull it, the more tightly it gets locked.[65]

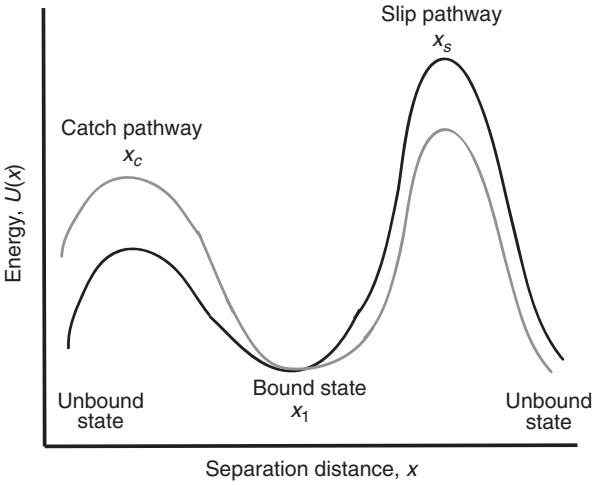

Figure 5 Potential energy profile for a one state two pathway dissociation model. The catch barrier has to be lower than the slip barrier for an efficient catch-slip transition to occur. The effect of force is described by the grey line. Modified, from Thomas, W. E.; Vogel, V.; Sokurenko, E. Biophysics of catch bonds. Annu Rev Biophys, **2008**, *37*, 399–416. Copyright by Annual Review.

7.3.4.2 Physical and Mathematical Descriptions of the Two-Pathway Model

Physical and mathematical models were proposed to describe published experimental data showing that selectin–ligand bonds exhibit catch and slip bond behavior. To account for this, two-pathway dissociation models were developed. Conceptually, the receptor–ligand bond can be imagined to be shaped like a harpoon or a hook. This configuration can lock 'tightly' when pulled apart by the two ends. Hence, the unbinding time (or bond lifetime) increases with the applied force initially, reflective of the catch bond behavior. Progressively increasing forces are responsible for bending the elastic hook and promoting dissociation through the slip pathway.[71] Alternatively, the receptor can undergo a ligand-induced switch to an active conformation.[71] The transition state in the catch pathway would be a reversion to the inactive conformation followed by immediate receptor–ligand unbinding. The slip pathway would involve unbinding through the active conformation, equivalent to the forceful bending of the elastic hook.

A simple four-parameter model[72] describes the unbinding of the selectin–ligand complex from a single bound state either along the catch-bond pathway over a low-energy barrier or the slip-bond pathway over a high-energy barrier (**Figure 5**). In the absence of an external force, the transition of the receptor–ligand complex from the bound state to the free state is related to the thermal probability of reaching the top of the barrier. The unbinding rate is exponentially dependent on the depth of the energy barrier ΔE_0:

$$k_{12}^0 \sim e^{-\Delta E_0/k_B T} \quad [32]$$

The effect of external force on the bond can be represented by considering the change in the height of the energy barrier ΔE:

$$\Delta E = \Delta E_0 - x_{12} f \quad [33]$$

where $x_{12} = |\overrightarrow{x_2} - \overrightarrow{x_1}|\cos\theta$, is the distance between the bound state 1, and the transition state 2 projected on to the direction of the externally applied force f. θ is the angle between the directions of the force and the displacement of the ligand from x_1 to x_2. The receptor–ligand complex forms a slip bond when the applied tensile force pulls the bond from the bound state to the transition state by performing positive work on the ligand, thereby lowering the energy barrier (**Figure 5**). The projected distance is positive ($x_{12} > 0$). Hence, the bond breakage in this case is through a single pathway. But force can also pull the ligand away from the transition state in such a way that the projected distance becomes negative ($x_{12} < 0$). In this situation, the force performs negative work on the ligand and increases the depth of the energy barrier ΔE, thereby decreasing the dissociation rate (**Figure 5**). In other words, the applied tensile force increases the lifetime of the receptor–ligand bound complex and makes it a catch bond.[65,72]

For a catch-slip transition to occur, the bound complex should be able to dissociate from the bound state via two alternative paths that can be available. They can be represented as two finite energy barriers on either side of the bound state. The probability that a ligand is still bound to its receptor at a later time $t > 0$ is given by $P(t)$. This probability decreases with time according to the equation:[72]

$$\frac{dP}{dt} = -(k_{1c} + k_{1s})P(t) \quad [34]$$

where k_{1c} and k_{1s} are the dissociation rate constants for unbinding through the catch and slip pathways with the coordinates x_c and x_s, respectively.

The dissociation rates along with catch and slip pathways depend exponentially on the applied force according to the

following relations:

$$k_{1c} = k_{1c}^0 \exp\left(\frac{x_{1c} f}{k_B T}\right); \quad k_{1s} = k_{1s}^0 \exp\left(\frac{x_{1s} f}{k_B T}\right) \qquad [35; 36]$$

where k_{1c}^0 and k_{1s}^0 are the unstressed dissociation rates along the catch and slip pathways respectively. x_{1c} and x_{1s} are given by $x_{1c} = -|\vec{x_c} - \vec{x_1}|\cos\theta < 0$; $x_{1s} = |\vec{x_s} - \vec{x_1}|\cos\theta > 0$. The solution to the equation for the survival probability is $P(t) = \exp[-(k_{1c} + k_{1s})t]$, which implies that the two pathway model arising from a single bound state displays a single exponential decay. The inverse mean lifetime of the bound state is given by:

$$\frac{1}{\tau(f)} = k_{1c}^0 \exp\left(\frac{x_{1c} f}{k_B T}\right) + k_{1s}^0 \exp\left(\frac{x_{1s} f}{k_B T}\right) \qquad [37]$$

When the applied external force increases from zero, the lifetime of the bond increases until a maximum value is reached at a critical force. Within this force regime, the receptor–ligand bonds possess a unique ability to exhibit longer lifetimes under force, which is reflective of the catch bond behavior. This can be achieved if k_{1c} decreases more rapidly than k_{1s} increases in the low force regime. Above the critical force, the slip pathway dominates so a continued increase in force would accelerate dissociation by suppressing the energy barrier.

Using this model, the four parameters, namely, k_{1c}^o, k_{1s}^o, x_{1c} and x_{1s}, were estimated for previously published experimental P-selectin-PSGL-1 data to be: $k_{1s}^o = 0.25 \pm 0.05\ s^{-1}$, $x_{1s} = 5.1 \pm 0.5$ Å; $k_{1c}^o = 120 \pm 55\ s^{-1}$, $x_{1c} = -21.7 \pm 2.4$ Å[72], and found to be in good agreement with MFP data[12].

Another two-pathway model was described by Evans and colleagues[42]. In this model, the receptor–ligand bond can dissociate along two force dependent pathways from two bound states, which are in thermal equilibrium with each other. The authors assumed a rapid inner conversion between the two states, which reduced the model parameters from nine to five. The switch from the low impedance pathway (which has a fast dissociation rate) to the high impedance pathway (which has a slow dissociation rate) by the application of force is governed by the change in the occupancies of the two bound states, and this determines the transition from catch to slip bond behavior.[42] P-selectin-PSGL-1 was found to act as a mechanochemical switch where the force history determines the pathway along which the receptor–ligand complex dissociates.[42] The authors tested this hypothesis using a novel jump/ramp mode of force spectroscopy.[42]

7.3.4.3 Experimental Demonstration of Selectin–Ligand Catch-to-Slip Bond Transition

Zhu and colleagues provided the first experimental observation of catch bonds involving selectins using force spectroscopy and flow-chamber experiments. The dependence of bond lifetimes on applied tensile force for P-selectin-PSGL-1 interactions was directly measured by force spectroscopy.[45] In these experiments, the dimeric form of PSGL-1 or the monomeric recombinant soluble PSGL-1 (sPSGL-1) immobilized on the cantilever was brought repeatedly in contact with P-selectin incorporated into polymer supported lipid bilayers. After applying a constant force to the P-selectin-PSGL-1 bond, its lifetime was recorded (**Figure 6(a)**). For a given force, the logarithm of the number of events that survived was also plotted against the lifetime t (**Figure 6(b)**). When the lifetime of the bond was measured and plotted against all applied forces, it was observed that it initially increased at low forces, indicative of the catch bond behavior (**Figure 6(a)**). At higher forces, the bond lifetime decreased, indicative of the traditional slip bond behavior (**Figure 6(a)**). This produced a characteristic biphasic pattern depicting the transition of the catch bond to slip bond when a certain critical force level is reached (**Figure 6(a)**).[45]

Interestingly, the lifetimes and critical force for P-selectin–dimeric PSGL-1 interactions were approximately double in comparison to those for P-selectin-sPSGL-1 interactions (**Figure 6(a)**). Hence, their data suggest that sPSGL-1 forms monomeric bonds with P-selectin, whereas the native form of PSGL-1 forms dimeric bonds with P-selectin[45]. The dimeric bond was able to withstand higher tensile forces and exhibit

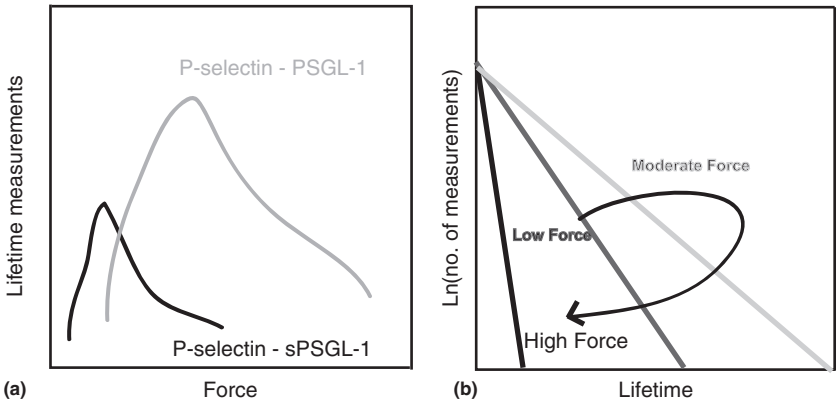

Figure 6 (a) Measurements of bond lifetimes between P-selectin and monomeric (sPSGL-1) versus dimeric PSGL-1 as a function of applied force. (b) The logarithm of the number of events that survived with increasing levels of force was plotted against the bond lifetime. These plots illustrate that P-selectin-PSGL-1 bonds exhibit catch bond behavior at low forces and transition to slip bonds at higher forces.

longer lifetimes, which explains the rightward and upward shifts, respectively, in the lifetime-force plot for P-selectin-dimeric PSGL-1 relative to P-selectin-sPSGL-1 interactions (**Figure 6(a)**). These force-spectroscopy data were confirmed by the use of flow chamber experiments[45].

L-selectin binding to its ligands, PSGL-1 and endoglycan, also displayed catch bond behavior at low forces and transition to slip bond in the higher force regime.[46] Molecular elasticity measurements revealed that the spring constants of L-selectin complexed with either dimeric PSGL-1 or sPSGL-1 were identical.[46] In stark contrast, the spring constant of P-selectin-dimeric PSGL-1 bond was twice that of P-selectin-sPSGL-1. Taken together, these data reveal that L-selectin is only capable of making monomeric bonds with PSGL-1.[46]

Independent experiments performed by Evans and colleagues[42] using a BFP with a combination of the 'steady ramp' and 'jump/ramp' modes of force spectroscopy also revealed that P-selectin-PSGL-1 bonds exhibit the catch-to-slip bond transition.

7.3.4.4 Structural Basis of Selectin–Ligand Catch-Slip Bonds

High affinity binding of the lectin domain of P-selectin to PSGL-1 requires three clustered tyrosine sulfate residues, adjacent peptide components, fucose and sialic acid residues on an optimally positioned short core-2 O-glycan within the anionic N-terminal region of PSGL-1.[5,10] All of these moieties have a distinct contribution to the binding affinity of PSGL-1 to P-selectin, and must be presented in a stereochemically precise configuration for optimal binding that also involves a combination of electrostatic and hydrophobic contacts. Somers et al. showed that the sulfotyrosine-containing region of PSGL-1 binds P-selectin in an area of positive electrostatic potential whereas its sialic acid/fucose component interacts with P-selectin in a region of neutral and negative electrostatic potential.[5] Based on the structural information of P-selectin bound to PSGL-1 derived glycosulfopeptide and in light of reports suggesting that the EGF-like domain of the P-selectin molecule may regulate its function in various ways,[5] a model was speculated[73] to explain catch and catch-slip transitional bond behavior of P-selectin-PSGL-1 complex *in vivo*. Mechanical forces induce a conformational change at the interface of the lectin and EGF domains of P-selectin that propagates along the lectin domain ultimately triggering the PSGL-1 binding site to change from a low affinity to a high affinity conformational state[73]. These changes in the binding affinity may manifest in the well known catch bond behavior. Comparison of crystal structures of uncomplexed P-selectin and P-selectin-ligand complex at equilibrium reveals that the largest change in the P-selectin conformation occurs at the interface of the lectin and EGF-like domains, whereas small structural changes are evident in the putative PSGL-1 binding site.[5] Mechanical forces could also elongate the flexible PSGL-1 molecule, and thus better expose its critical determinant for recognition by P-selectin.[73] Weak P-selectin-PSGL-1 interactions induced by low hemodynamic forces may be mediated by either the sialyl Lewis x present on a short core-2 O-glycan or any of the sulfotyrosine residues. Increasing hemodynamic forces may strengthen binding (catch bond behavior) by inducing conformational changes in the binding pocket that ultimately present the critical binding determinants on both P-selectin and PSGL-1 in a proper configuration for cooperative binding.[73] These structural changes may result from the exposure of buried residues in the binding pocket, resulting in newer opportunities for attractive interactions, which would prolong the lifetime of the bond. Alternatively, if the pathway to debonding involves the deformation of compliant domains distal from the binding pocket, then application of a force may retard the rate of deformation, thereby augmenting the stability of the P-selectin-PSGL-1 bond. When the force crosses a critical threshold value, all the electrostatic and hydrophobic interactions between P-selectin and PSGL-1 are disrupted and the lifetime decreases leading to the slip bond regime.[73]

The above model[73] was validated and extended by molecular dynamics simulations, Monte Carlo modeling, and mutational experimental studies by laying emphasis on the angle between the lectin domain and the EGF-like domain of the selectin molecule.[74,75] Molecular simulations reveal that the structure of P-selectin liganded with PSGL-1 yielded an interdomain angle of 139.3° in the open-angle conformation, whereas that of P-selectin liganded with sLe^x had an interdomain angle of 114.6° in the closed-angle conformation.[75] When tensile force is applied to the selectin–ligand complex, there is a greater probability for the selectin to exist in the open angle conformation.[74] Taking into account the noncovalent interactions at the atomic level, molecular dynamics simulations of P-selectin unbinding from PSGL-1 showed that the interdomain angle opening allows rotation of the lectin domain and makes the binding interface tilt and align itself better with the direction of force.[75] This results in sliding of the ligand along the binding interface as the preexisting interactions dissociate. This provides opportunity for newly formed interactions between the two sides of the interface, which replace those that have already dissociated, thereby bringing the system back to its previously bound state. This prolongs the lifetimes by slowing dissociation, resulting in catch bonds. Four residues on the PSGL-1 glycan: fucose, sialic acid, galactose, N-acetylglucosamine and eight residues from the PSGL-1 peptide including three sulfated tyrosines were observed to form new interactions most frequently.[75] Thus, a flexible hinge between the lectin and EGF-like domain allows mechanical force to allosterically cause catch bond with the selectin ligand via sliding-rebinding mechanism. Once the interdomain angle is fully open, the probability for rebinding becomes maximum. Further increase in applied force will not increase the lifetimes, instead it will accelerate the dissociation resulting in the catch-to-slip bond transition.[75]

It is noteworthy that the P-selectin's hinge between the lectin and EGF-like domain is more flexible than that of L-selectin.[74] This physical property appears to account for the longer lifetime of P-selectin–ligand catch bonds that convert to slip bonds at lower forces than L-selectin. The force required to place the equilibrium between the closed and the open angle conformation is greater for L-selectin than P-selectin primarily because of the presence of a hydrogen bond between the residues Tyr37 and Asn138.[74] The frequency of transition

between the closed and the open angle conformation increases with increasing the flexibility of the hinge. By eliminating the hydrogen bond between Tyr37 and Asn138 by mutational experiments, the rotational diffusivity of the lectin domain of L-selectin increased, which resulted in increased tethering of L-selectin-bearing microspheres on PSGL-1-coated substrates.[74] Taken together, the increased bond formation rate and the longer lifetime of catch bonds at lower forces as a result of the increase in the flexibility of the L-selectin hinge were found to lower the shear threshold for L-selectin dependent rolling.

7.3.4.5 Physiological Significance of Catch-Slip Bonds

Catch bonds have been shown to regulate the flow-enhanced leukocyte adhesion to selectin-coated surfaces in experimental[66] and simulation[76,77] studies. Both L-selectin and PSGL-1 are expressed on the surface of circulating leukocytes, and have been reported to play a key role in homotypic leukocyte adhesive interactions in shear flow.[78,79] Without the catch bonds to shorten the bond lifetimes at low shear stresses, spontaneous homotypic aggregation of free-flowing leukocytes via an L-selectin-PSGL-1-dependent mechanism would be induced with unwanted clinical manifestations. Hence, the catch bonds function to prevent leukocyte aggregation when it is not needed.[80] Understanding the catch bond behavior will help us to redesign novel catch bonds for medical/therapeutic purposes and for engineering structures that can be used for various technological applications, inspired by this naturally occurring phenomenon.

7.3.5 Selectin-Mediated Cell Adhesion in Shear Flow

Cell adhesion mediated by biological macromolecules and their respective ligands plays a key role in a number of diverse biological phenomena including inflammation and cancer metastasis. Leukocyte recruitment to sites of infection is regulated by highly specific receptor–ligand interactions that allow leukocytes to first tether and roll on activated endothelium under hydrodynamic shear and then firmly adhere prior to their extravasation into the tissue space. Accumulating evidence suggests that tumor cell arrest in the microcirculation is also mediated through receptor–ligand interactions between tumor cells and the vascular endothelium in a manner analogous to leukocyte recruitment.[81–84] Both processes involve highly regulated molecular events such as selectin–ligand interactions that rely on the local circulatory hemodynamics and the mechanical and kinetic properties of participating adhesive molecular groups. Providing sufficient observation capabilities and mimicking the physiological flow environment, flow chamber assays have been utilized to study selectin-mediated cell binding.[38,39,66,85] This section discusses how flow modulates the binding of a cell to a functionalized surface, focusing on theoretical, experimental, and numerical studies reported in the literature.

7.3.5.1 Mathematical Description of Cell Tethering to a Selectin-Coated Surface in Couette Flow

In flow-based adhesion assays, the translational velocity at any given instant describes different types of cell motion.[86,87] Specifically, a cell is in free motion when its translational velocity is close to the prevailing hydrodynamic velocity. When the cell mean velocity is significantly slower than the hydrodynamic velocity due to the formation/dissociation of receptor–ligand bonds, the cell is classified as in rolling motion. If a cell is stationary for at least several seconds, it is considered as firmly-adherent. Although cell rolling is a complex process controlled by many different physical and chemical parameters such as cell deformation, microvillus extension, receptor and ligand densities, and receptor–ligand bond formation and dissociation, several simplifications can still be made. In the low shear regime, the cell deformation can be neglected such that the cell can be modeled as a hard sphere in a Couette flow.[88] If ligands are immobilized on the substrate at very low site densities, the binding interaction can be assumed to involve a single receptor–ligand bond complex. Therefore, the bond lifetime can be obtained by simply recording the cell tethering time. Here, we discuss the suitability of the Couette flow assumption. Then, a physical model will be discussed to estimate the bond rupture force induced by the hydrodynamic shear.

The diameter of blood cells, for example leukocytes, varies from 6–10 μm, and as such, viscous effects dominate the flow behavior as characterized by a small Reynolds number, typically much smaller than unity. Thus, the flow is laminar, and is described by the Stokes flow equation. The flow field u can be assumed as 2-D, as shown in **Figure 7(a)**, since most of flow chambers have a width much bigger than the height (about 10 times in ratio). If cells are rolling close to the bottom wall with a distance much smaller than the height of flow chamber, the flow velocity profile in the vicinity of the channel bottom surface can be approximated to be linear (Couette flow), as depicted in **Figure 7(b)**. This linear approximation significantly simplifies the analysis of cell-surface adhesive interactions.

An exact solution has been derived for a neutrally buoyant sphere moving next to the wall by an imposed Couette flow.[88] Although cells are not neutrally buoyant due to slight differences in their density relative to that of the suspended buffer, they can be considered as "neutrally buoyant" because the gravitational force keeps them only rolling along the bottom wall and eliminates their cross-streamwise motion. Hence, the exact solutions apply in this situation. The equations to calculate shear-induced force and torque are given by:

$$F_x = 1.7005 \times \left(6\pi\mu R^2 S\right) \quad [38]$$

$$T_y = 0.944 \times \left(4\pi\mu R^3 S\right) \quad [39]$$

where μ is the viscosity of the suspended buffer, R is the radius of cell and S is the shear rate. The values inside parentheses represent the shear-induced force and torque without having a wall next to the cell. The wall effect induces 70% greater force and 5.6% less torque onto the rolling cell. The bond rupture

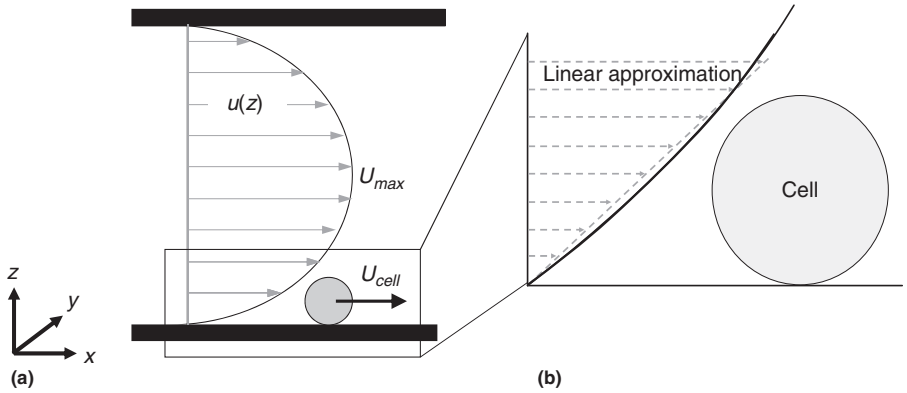

Figure 7 (a) The 2-D fully-developed flow velocity profile is only the function of cross-streamwise direction *z*. (b) Comparison between the actual flow velocity profile (black curve) and the linear approximation (gray dotted line) for a short distance closed to the wall.

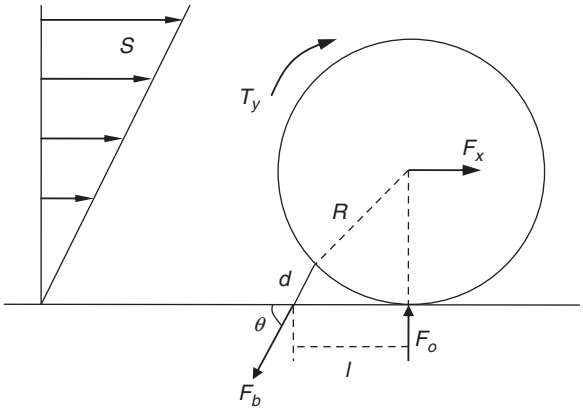

Figure 8 Force balance on a tethered cell in shear flow. Fluid shear rate S will induce a force F_x and torque T_y on a cell of radius R. A tether which has length d and oriented at an angle θ with the substrate experiences a force F_b. The binding point between the cell and the surface locates l distance from the projection of the center of cell.

force can be estimated by balancing forces and torques on the cell at static equilibrium as depicted in **Figure 8**. Assuming that there is only one bond capturing the rigid spherical cell (**Figure 8**), then the sum of forces in x or z-direction must equal zero at static equilibrium:

$$F_x = F_b \cos\theta \quad [40]$$

$$F_o = F_b \sin\theta \quad [41]$$

The sum of torque in y-direction about the contact point of F_o is given by:

$$T_y + F_x R = l \cdot (F_b \sin\theta) \quad [42]$$

where the length of lever arm l, equals the distance between the binding point and the contact point of F_o (**Figure 8**). The lever arm can be determined by measuring the distance that bound cells move during flow reversal assays[38,89]. The tether length d (**Figure 8**) can be estimated by the total length of an extended microvillus and the selectin molecules.[38,89,90] The oriented angle θ of the tether is expressed by[90]:

$$\theta = \tan^{-1}\left(\frac{R}{l}\right) + \cos^{-1}\left(\frac{d^2 + l^2}{2d\sqrt{R^2 + l^2}}\right) \quad [43]$$

The parameters of neutrophils and HL-60 human promyelocytic cells are listed in **Table 5**. Although the F_b/F_x ratios are similar between these two cell types, HL-60 cells experience about a 2-fold larger hydrodynamic force because of their larger cell diameter relative to neutrophils, as disclosed by eqn [38].

7.3.5.2 Estimation of Selectin–Ligand Bond Dissociation Rates From Flow Chamber Assays

In flow-based adhesion assays, cells pause for short periods of time (t_b) and then translate forward in the direction of flow as shown in **Figure 9(a)**. The pause time, t_b, is the bond lifetime, and the dissociation kinetics can be obtained by quantifying its distribution. Due to the probabilistic nature of receptor–ligand bond rupture, the fraction of bound cells will decrease exponentially with time under a constant force.[91] By plotting the natural logarithm of the number of cells that remained bound as function of lifetime, the dissociation rate k_r can be obtained by the negative slope of the fitting curve as shown in **Figure 9(b)**.[38,64] After repeating the flow assays at different wall shear stresses, the estimated dissociation rates can be plotted as a function of applied force, which is calculated from eqns [40]–[43]. The values of k_r^0 and x_β will be estimated by fitting dissociation rates with the Bell model as shown in **Figure 9(c)**.[38,39,64,89] To ensure that this analysis will yield the binding kinetics of a single receptor–ligand pair, experiments are performed at very low selectin site densities on the substrate; typically, lower than those supporting stable leukocyte rolling. Moreover, the independence of cellular dissociation rate on the selectin density is indicative that a monovalent bond between the selectin molecule and its ligand has been identified.[64] This analysis has also been used to detect the catch bond behavior of selectin–ligand bonds at low applied forces.[45]

Table 5 Model parameters reported in the literature for neutrophil and HL-60 cell tethering to selectin-coated surfaces.

Cell	*R* (μm)	*d* (μm)	*l* (μm)	θ ($^\circ$)	F_b/F_x
Neutrophil	4.25 $\pm$ 0.24	1.0 $\pm$ 0.2	3.0 $\pm$ 0.38	62.8 $\pm$ 1.9	2.18 $\pm$ 0.13
HL-60	6.3 $\pm$ 0.8	1.6 $\pm$ 0.5	4.7 $\pm$ 1.0	61.5 $\pm$ 2.5	2.09 $\pm$ 0.19

Alon, R.; Chen, S.; Puri, K. D.; Finger, E. B.; Springer, T. A. The kinetics of L-selectin tethers and the mechanics of selectin-mediated rolling. *J. Cell. Biol.* **1997**, *138*(5), 1169–1180. Smith, M. J.; Berg, E. L.; Lawrence, M. B. A direct comparison of selectin-mediated transient, adhesive events using high temporal resolution. *Biophys. J.* **1999**, *77*(6), 3371–3383. Chen, S.; Alon, R.; Fuhlbrigge, R. C.; Springer, T. A. Rolling and transient tethering of leukocytes on antibodies reveal specializations of selectins. *Proc. Natl. Acad. Sci. U S A* **1997**, *94*(7), 3172–3177.

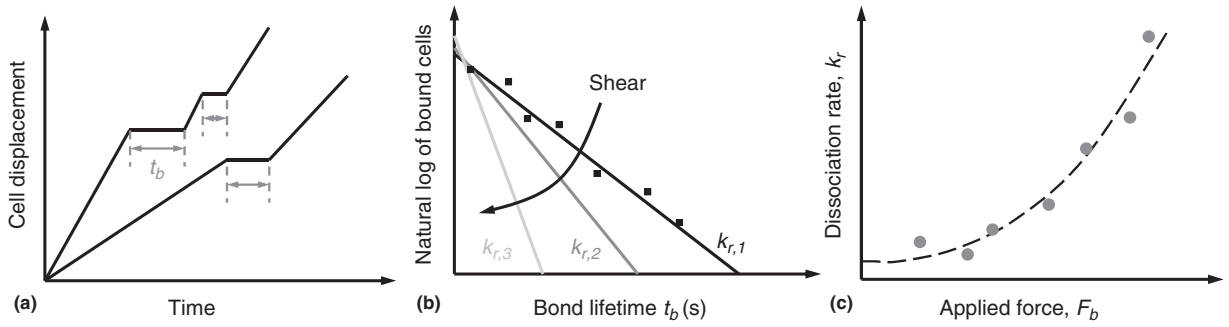

Figure 9 (a) Displacement-time schematic of leukocyte rolling on a selectin-coated surface. The durations of transient tether events marked by the double arrows represent the selectin–ligand bond lifetime t_b under shear. (b) The distribution of bond lifetimes measured from a displacement-time plot. The fitting slope represents bond dissociation rate k_r. (c) Dissociation rates as a function of applied force. The values of unstressed dissociation rate k_r^0 and reactive compliance x_β can be estimated by fitting the Bell model with data points.

During inflammation, leukocytes tether and roll on activated endothelium via formation of specific selectin–ligand bonds. Although all three selectins have similar molecular structures, neutrophils roll markedly faster on L-selectin relative to P- and E-selectins.[92] By measuring bond lifetimes,[38] showed that the $k_r(f)$ for L-selectin is larger than that of P- and E-selectin for bond forces ranging from 40 to 240 pN. By extrapolating k_r to zero rupture force, the unstressed dissociation rates k_r^0 of L-selectin was found to be 7–10 times larger than that of P- and E-selectin.[37,38] When the force exerted on the bond increases, Ref. 38 showed that the dissociation rate increases less for L-selectin than for P- and E-selectin. Therefore, these authors hypothesized that the faster neutrophil rolling on L-selectin is mainly due to the higher unstressed dissociation rate. The reactive compliance, which represents susceptibility of bond dissociation to the applied force, is not responsible for the faster rolling.[38]

However, mathematical models of leukocyte rolling suggest that the reactive compliance correlates positively with rolling velocity;[91,93] that is, the higher the reactive compliance the faster the cell rolling. It is noteworthy that under high shear, the cell pause times due to L-selectin-dependent tethering may be on the order of standard video capture rates.[39] To address this issue, Lawrence and colleagues[39] employed high-speed videomicroscopy to record the lifetime of neutrophil–selectin bonds under flow. Their analysis revealed that the lifetimes of L-selectin–ligand bonds are drastically shorter than those of P- and E-selectin–ligand ones, and highly compliant to applied force. The reactive compliance of L-selectin-ligand bonds obtained with the high-speed camera is larger than that of E-/P-selectin–ligand bonds.[39] Smith et al. also indicated that a significant amount of binding and dissociation events were not detected by the standard camera, and as such the L-selectin–ligand reactive compliance was underestimated in experiments recorded by standard video capture rates. The data obtained by high-speed videomicroscopy are in qualitative agreement with the single-molecule force microscopy results discussed in section 7.3.3.3.[12]

7.3.5.3 Shear-Controlled Association Rate

The free motion of a neutrally buoyant sphere (e.g., modeled leukocyte) near a wall in a shear field has been studied analytically and numerically by an image representation method and series expansions.[88,94,95] If there were no viscous fluid moving around the sphere, its translational velocity U_{cell} would be synchronized with angular velocity Ω when the sphere is in the limit of touching the surface; this situation can be envisioned when someone is rolling a basketball on the floor. Hence, $R\Omega/U_{cell}$ would be equal to unity. However, the sphere will experience a different motion under the influence of a viscous flow. If the coordinate z is defined as the position of sphere centered above the wall, the gap distance is then equal to $(z–R)$ where R is cell radius. The numerical solutions of $R\Omega/U_{cell}$ obtained by Goldman[88] are plotted against the normalized gap distance $(z–R)/R$ as shown in **Figure 10**. Interestingly, when the gap distance approaches zero, $(z–R)\rightarrow 0$, the value of $R\Omega/U_{cell}$ does not approach unity but a finite limit at about 0.5676. Therefore,

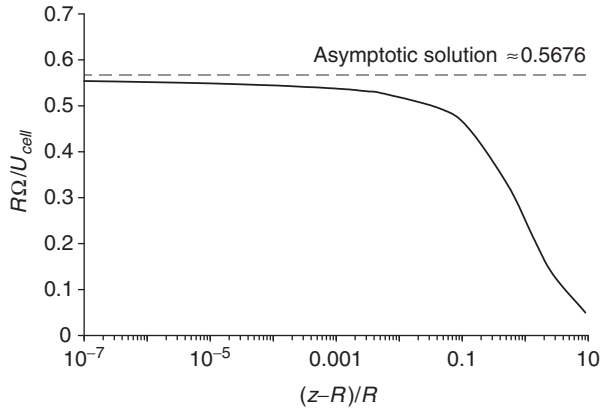

Figure 10 The ratio $R\Omega/U_{cell}$ is given as function of the normalized gap distance $(z\text{-}R)/R$. The asymptotic solution indicates that the translational velocity is not synchronized with the angular velocity when a cell is in close proximity with a wall. From Goldman, A. J.; Cox, R. G.; Brenner, H. Slow Viscous Motion of a Sphere Parallel to a Plane Wall .2. Couette Flow. *Chem. Eng. Sci.*, 1967, *22*(4), 653–660.

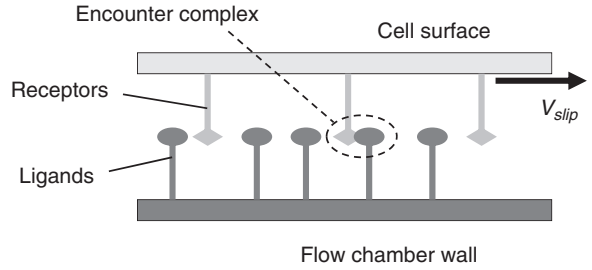

Figure 11 Schematic diagram showing that the cell slipping velocity increases the encounter rate of membranebound receptors and immobilized ligands on the substrate. Compared to the static condition that only allows receptors to react with their adjacent ligands, the finite slipping velocity can enhance the receptor–ligand association rate.

the translational velocity U_{cell} is always larger than the surface tangential velocity $R\Omega$, leading to a cell slipping motion relative to the flow chamber wall. This slipping velocity can be expressed by:

$$V_{slip} = U_{cell} - R\Omega \quad [44]$$

$$V_{slip} \approx U_{cell} - 0.5676 \cdot U_{cell} \approx 0.4324 \cdot U_{cell} \quad [45]$$

This unique slipping velocity increases the encounter rate between a receptor and a ligand[96] (**Figure 11**). If there is no slipping motion between the cell surface and the chamber wall, each cell receptor can only interact with a limited number of ligands located within its reactive zone. In contrast, when a cell surface is moving with a finite slipping velocity, each cell receptor can react with any ligand passing by its reactive zone. Therefore, the overall cell binding can be enhanced by increasing the flow rate due to the shear-enhanced association rate.[76,96]

The process to establish a successful receptor–ligand bond can be divided into two steps: encounter and reaction.[60] If V_{slip} is sufficiently small, the major encounter mechanism will be controlled by the diffusivity of receptors and ligands on their respective surfaces. Thus, the encounter rate k_0 has a diffusive and a convective limit characterized by Péclet number:[76,96]

$$k_0 = \begin{cases} \dfrac{2\pi D}{\ln(b/a)} & \mathrm{Pe} \ll 1 \\ 2D\mathrm{Pe} & \mathrm{Pe} \ll 1 \end{cases} \quad [46]$$

where D is the relative diffusion coefficient, which equals the sum of the surface self-diffusivities for the target receptor and ligand, a is the radius of the reactive circle around the receptor, b is half of the mean distance between the ligand molecules, and the Péclet number is defined by $\mathrm{Pe} = V_{slip}a/D$. The first equation in [46] calculates the encounter rate at the diffusion limit, whereas the second is at the convection limit. When a free ligand is brought inside the reactive circle of a receptor, this complex will start to react. The original model proposed by Chang[96] assumes that an encountered complex is always possible to react, such that the bond association rate is always enhanced by the cell slipping velocity. However, the successful formation of a bond also depends on the encounter duration between these two molecules. Caputo[76] introduced a timescale $(1/\nu)$ for exploring the conformational space, which represents the minimum required time for bond reaction. So, if the encounter duration is shorter than this timescale, the probability of bond formation is set to zero. The shear-controlled association rate is given by:

$$k_f = k_0 P \rho_L \quad [47]$$

where ρ_L is the density of adhesive molecules on the substrate surface, P is the probability of reaction, and its detailed expression for both diffusive and convective limits is described by Chang[96] and Caputo[76]. If the number of available receptors is constant inside the cell-surface contact region, the theoretical overall cell adhesion rate can be calculated by the following equation:[96]

$$k_{ad} = k_f N_r \quad [48]$$

where N_r is the number of effective receptors inside the cell-surface contact region. The proposed model successfully includes the shear flow effect in determining the association between a cell receptor and a surface ligand. Since the rate of encounter between adhesion molecules increases with the V_{slip}, the shear-controlled association rate may explain, at least partly, the counterintuitive shear threshold phenomenon reported for selectin-mediated cell rolling.[67,68]

7.3.5.4 Shear Threshold Phenomenon of Selectin-mediated Cell Rolling

Selectins require a shear threshold to mediate optimal leukocyte tethering and rolling.[67,68] In other words, leukocyte tethering first increases and then decreases while monotonically increasing the wall shear stress (**Figure 12**). This phenomenon seems counterintuitive because increasing levels of shear stress increase the dislodging force on the cell, thereby increasing their probability to detach from the substrate. However, both *in vitro* and *in vivo* assays reveal that the shear

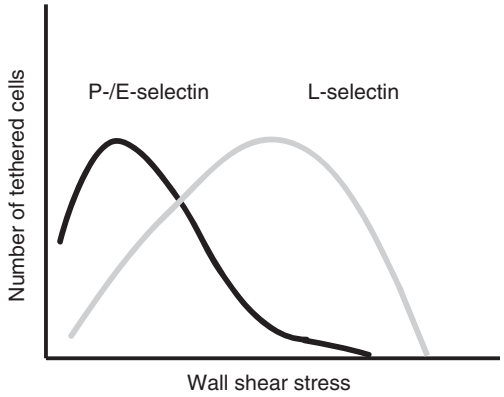

Figure 12 Schematic plot illustrating the shear threshold phenomenon observed for P-, E- and L-selectin-mediated adhesion. The number of tethered cells increases until a critical shear stress level is reached, beyond which it decreases. The shear stress threshold reported for L-selectin (0.8 dyn/cm^2) is higher than those for E- and P-selectin (0.5 dyn/cm^2).

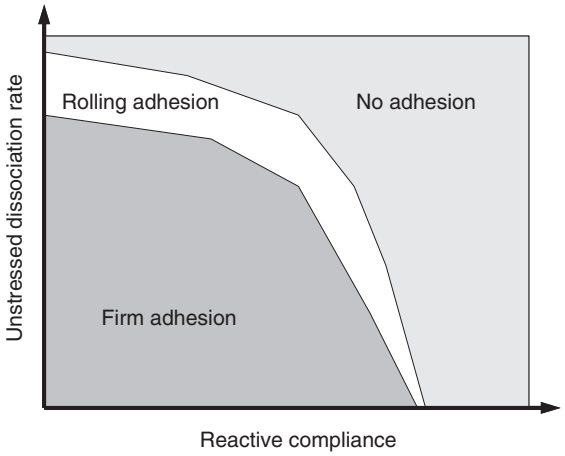

Figure 13 The Adhesive Dynamics state diagram indicates that the cell rolling motion is characterized by the two major Bell model parameters, the unstressed dissociation rate and the reactive compliance. Four adhesive regions, termed as firm adhesion, transient adhesion, fast adhesion and no adhesion, have been identified. The Bell model parameters of all three selectins fall in the rolling adhesion region. Adapted with permission from Chang, K. C.; Tees, D. F.; Hammer, D. A. The state diagram for cell adhesion under flow: leukocyte rolling and firm adhesion. *Proc. Natl. Acad. Sci. U S A*, **2000**, *97*(21), 11262–11267. Copyright by PNAS.

threshold phenomenon may be characteristic of the binding of all three selectins to their respective glycoprotein ligands.[67,68]

Shear-induced cell deformation was initially suggested to contribute to this phenomenon by increasing the contact area between the cell and the substrate and thus the probability of selectin–ligand bond formation under shear.[68] However, simulation studies reveal only a modest role for cell deformation in the shear-threshold phenomenon.[77] In view of observations showing that cell-free flow assays using purified selectins and their respective ligands can successfully recapitulate the shear-threshold phenomenon,[45,66] it is now widely believed that the origin of this phenomenon is predominantly molecular, intimately associated with the kinetic and micromechanical properties of selectin–ligand bonds.

By analyzing the various biophysical parameters that govern selectin-mediated adhesion under flow, Zhu and colleagues identified two principal mechanisms that contribute to the flow-enhanced leukocyte adhesion to selectins:[97] transport-dependent acceleration of bond formation and force-dependent deceleration of bond dissociation. Selectin-mediated cell tethering is enhanced by three distinct modes of transport, as shown by dimensional analysis:[97] (i) the relative sliding between the cell and the surface; (ii) the Brownian motion, which alters the gap distance between the cell and the surface and increases their collisions; and (iii) the molecular diffusivity of the receptors and ligands, which orients their binding sites for molecular docking. The second mechanism refers to the selectin–ligand catch bonds, where tether force prolongs their lifetime. Interestingly, simulation studies using the adhesive dynamics model for cell rolling disclose that the shear-threshold phenomenon is best achieved by a catch–slip bond and to a lesser extent by the shear-controlled on rate.[76] Dimensional analysis studies reveal that the tether force, but not wall shear rate or wall shear stress, is the dominant parameter governing flow-enhanced cell rolling.[97] Taken together, experimental and simulation studies collectively show that flow-enhanced leukocyte adhesion is caused by the mechanical regulation of the association and dissociation rates.

As discussed in section 7.3.4.4, using site-directed mutagenesis, it was reported that by increasing the flexibility of the L-selectin interdomain hinge, the tethering rate was increased due to enhanced rotational diffusion of L-selectin lectin domain and catch bonds displayed longer lifetimes at smaller forces. The mutated L-selectin with a more flexible hinge required a lower threshold shear for rolling, thus providing a structural explanation for this counterintuitive phenomenon.[74,75]

7.3.5.5 Numerical Simulations of Cell Rolling and Adhesion in Shear Flow

Computational studies, modeling leukocytes as hard-spheres, have systematically examined how the biophysical properties of cell adhesion molecules regulate cell rolling and firm adhesion.[76,86,87] Different cell adhesive behaviors have been observed in simulations, and related to the combinations of the Bell Model parameters k_r^0 and x_β, which were found to be the most important molecular properties governing the dynamics of cell adhesion. Hammer introduced a computational method called Adhesive Dynamics, by considering the formation and breakage of receptor–ligand bonds as stochastic events and by relating the dissociation to force and kinetic parameters.[86,91] The relationship between the Bell model parameters, k_r^0 and x_β, and various adhesive behaviors have been summarized in a state diagram shown in Figure 13.[86,87,98] The state diagram provides an understanding of the relationship between the functional properties of receptor–ligand bonds and the kind of adhesive behavior mediated by these bonds.

The diagram is separated into four regions: firm adhesion, transient adhesion (rolling), fast adhesion and no adhesion. For receptor–ligand pairs having a small unstressed dissociation rate, the cell binding is likely to be firm adhesion unless the reactive compliance is very large. Cell adhesion mediated by integrin molecules belong to this group. At the other extreme, if the receptor–ligand bond has a large unstressed dissociation rate and a large reactive compliance, the cells do not experience any adhesion and freely move under flow with velocities greater than 50% of the hydrodynamic velocity ($0.5V_H$).

There are two intermediate regions where the cell neither permanently adheres to the surface nor moves freely with the flow but undergoes transient and fast adhesions. In the region of fast adhesion, the velocity of the flowing cells gets reduced to 50% or less than the hydrodynamic velocity, but do not display any long-lasting arrests. In the region of transient adhesion, the cells show durable arrests. Rolling of leukocytes falls in the region of transient adhesion where the mean velocities are less than $0.5V_H$ and the cells exhibit extended arrests. The size of this region is small, such that only certain combinations of unstressed dissociation rate and reactive compliance result in the rolling adhesion. The constant velocity curve ($0.5V_H$) separates the region of no adhesion from fast adhesion. The region of transient adhesion is largely based on the fractional stop times of moving cells.

The state diagram successfully explains why the rolling is so unique and is only observed for a small group of cell adhesion molecules. If a receptor–ligand bond has a slightly higher reactive compliance than what it has for rolling behavior, it will fall into the region of no adhesion. Similarly, a slightly lower unstressed dissociation rate can switch the cell's adhesive behavior from rolling to firm adhesion. This numerical finding has been compared to experimental studies and shows that selectins have the combinations of k_r^0 and x_β, such that they are exactly located in this rolling adhesion region.[37–39,64,99]

Cellular responses to fluid shear stress depend intimately on the material properties and structure of the cell. Experiments involving cell indentation using atomic force microscopy as well as micropipette aspiration of cells have been previously conducted to estimate the mechanical properties of leukocytes.[100–102] Early rheological models approximated the leukocyte as a Newtonian viscous drop with a surface tension which provides it with the spherical shape.[100,101,103] However, a single set of parameters for these models was unable to predict the leukocyte rheology at both small and large deformation values determined by micropipette aspiration experiments. Moreover, experimental work has shown that the cortical tension of the leukocyte varies with the extent of deformability when the cell undergoes active deformation during phagocytosis.[104] To overcome this limitation, non-Newtonian drop models such as a shear thinning were proposed.[102,105] However, the aforementioned models have the drawback that they ignore the dual nature of the cytoplasms with its cytosolic and cytoskeletal phases. Dembo and colleagues have used a two-phase viscous drop model in which the cytoskeletal network and cytosol have different material properties.[106] Due to the axisymmetry of cell deformation during micropipette aspiration, it has been possible to map the 3-D problem to numerical simulations in 2-D space, thereby reducing computational expense. Nevertheless, this approach may not be appropriate for simulating the non-axisymmetric problems of cell–cell aggregation and cell rolling and adhesion to a substrate in a linear shear field.

Dong and coworkers have carried out the numerical simulation of cell rolling on a planar substrate in a fully developed Poiseuille flow in 2-D using the finite element method, where the cell is represented as an elastic ring enclosing an incompressible viscous fluid.[107,108] In this model, an energy balance was carried out to estimate the velocity of the rolling cell. The energy imparted to the cell by the flow field of the external (suspending) fluid is equal to the sum of (i) energy lost due to viscous dissipation in the internal (cytoplasmic) fluid and (ii) the energy utilized for the rupture of receptor–ligand bonds between the cell and the substrate.[107,108] Both extracellular and intracellular flow fields were solved using finite element methods. The Hookean spring model with a deterministic kinetic equation was used to simulate the receptor–ligand interactions under hydrodynamic force. The study revealed that as shear stress increases, an increase in cell–substrate contact area results in a larger dissipation of fluid energy to both adhesion bonds and viscous cytoplasm, whereas the fraction of fluid energy imparted to the cell decreases due to a flattened cell shape.[107,108] The model also predicted a plateau in leukocyte rolling velocity as shear stress further increased.[107,108] However, the model placed non-physical constraints on the contact area (contact length in 2-D) between the cell and substrate.[107,108] To overcome this limitation, N'Dri et al.,[109] used the IBM to develop a multiscale 2-D model of cell rolling which was coupled with a deterministic representation of the Hookean spring model of receptor–ligand interactions. In this study, the cell was modeled as a 2-D compound drop with the highly viscous inner core representing the cell nucleus. The study showed that the presence of a nucleus increased the bond lifetime, and decreased the cell rolling velocity. It further predicted that a cell with a larger diameter rolls faster with a reduced bond lifetime.[109] The model was able to predict bond lifetimes which were in close agreement with experimentally observed P-selectin-PSGL-1 bond lifetimes estimated during leukocyte tethering to surface immobilized platelets.[109,110] However, the model was not able to simulate the characteristic "stop and go" motion of rolling leukocytes due to the deterministic treatment of receptor–ligand binding kinetics. Moreover, the cell shapes predicted by the compound drop model at large deformations deviate from those experimentally observed. These deviations may be the direct outcome of modeling cell membrane as surface tension interface of a liquid drop rather than an elastic membrane, as recently suggested.[111]

A 3-D compound drop model simulating cell rolling in a parallel plate flow chamber was recently proposed in which the nucleus and cytoplasm were modeled as viscoelastic fluids.[112] The simulations indicate that at fixed wall shear stress values, the cell substrate contact area increases with increasing ratio of cell diameter to channel height. Moreover, under high shear rate conditions the cell forms an elongated structure similar to those tethers observed in leukocyte rolling experiments.[113] However, the deterministic kinetics of this model renders it incapable of simulating the 'stop and go'

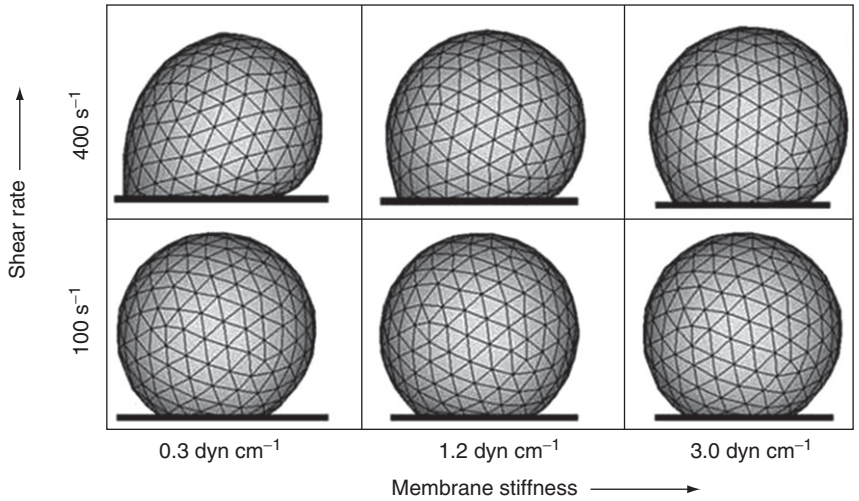

Figure 14 Numerical simulation of cell adhesion under shear flow. Receptor-mediated cell rolling was simulated using a 3-D computational model based on the immersed boundary method. Cell material properties such as membrane stiffness influence shear-induced cell deformation and cell substrate contact area. The representative cell shapes at shear rates of 100 and 400 s^{-1} are shown for membrane stiffness values of 0.3, 1.2 and 3.0 dyn/cm^2. Adapted from Jadhav, S.; Eggleton, C. D.; Konstantopoulos, K. A 3-D computational model predicts that cell deformation affects selectin-mediated leukocyte rolling. *Biophys. J.*, **2005**, *88*(1), 96–104.

rolling of leukocytes. Also, the high computational cost of the method limits the simulations to relatively short durations of leukocyte rolling. Moreover, like previous rheological models of the cell, the 3-D compound drop model does not account for the viscoelastic behavior of the microvilli.[113]

A 3-D computational model of leukocyte rolling was proposed to simulate receptor-mediated rolling of a deformable cell on a ligand-coated surface in a linear shear field.[114] The model parameters were chosen to represent PSGL-1-mediated leukocyte rolling on a P-selectin-decorated planar surface. In this model, the IBM[115] was used to simulate motion of an elastic capsule near a plane in a linear shear field. The IBM was coupled to the Hookean spring model to simulate the force-dependent kinetics of receptor–ligand interactions,[116] while the stochastic behavior of P-selectin-PSGL-1 bond formation and breakage was simulated by the Monte Carlo method.[86,91] The model successfully predicted that for a given shear rate, the extent of cell deformation and the cell-substrate contact area decreases with increasing cell membrane stiffness (**Figure 4**), and the rolling of more compliant cells is relatively smoother and slower compared to cells with stiffer membranes[114] which is in accord with experimental observations.[117,118] Moreover, the average number of bonds for a cell as well as those for a single microvillus was found to decrease with increasing values of membrane stiffness.[114] Along these lines, bond lifetimes decreased with increasing shear rate and also with increasing membrane stiffness.[114] More recently, Konstantopoulos and colleagues extended the aforementioned 3-D computational model to incorporate the three different kinetic models of receptor–ligand binding (e.g., Bell, Dembo and two-pathway model) and to account for microvillus deformability.[77] These simulations predicted that the catch–slip bond behavior and to a lesser extent bulk cell deformation contribute to the shear-threshold phenomenon. Cells bearing deformable rather than rigid microvilli roll slower only at high P-selectin site densities and elevated levels of shear ($\geq 400\ s^{-1}$). Further development of the mechanical models of biological cell structure is still required; however, the relative simplicity of these models can be advantageously employed to determine the influence of individual physical mechanism on cellular adhesion efficiency (**Figure 14**).

7.3.6 Conclusion

A detailed understanding of the biophysical nature of selectin–ligand interactions pertinent to the inflammation and cancer metastasis is essential for developing promising therapies and/or diagnostic tools to combat these disorders. Fluid (blood) flow influences cell adhesion at the mesoscale by affecting the mechanical response of cell membrane and the intercellular contact area, and at the nanoscale level by modulating the kinetics and mechanics of receptor–ligand interactions. Consequently, elucidating the molecular and biophysical nature of cell adhesion requires a multidisciplinary approach involving the synthesis of fundamentals from hydrodynamic flow, molecular kinetics and cell mechanics with biochemistry/molecular cell biology. Progress in each of the aforementioned research areas is key to the development of mathematical models of cell adhesion that incorporate the appropriate biological, kinetic and mechanical parameters that would lead to reliable qualitative and quantitative predictions. The ability to accurately predict receptor–ligand binding will be vital to the determination and optimization of important design parameters such as density, affinity and tensile strength of targeting receptor–ligand

interaction, for developing effective drug carriers for delivery of therapeutic agents to the afflicted sites of the host.

Acknowledgments

This work was supported by NIH/NCI R01 CA101135, U54 CA143868 (to K.K. and D.W.), a Predoctoral Fellowship (to P.S.R) and a Postdoctoral Fellowship (to L.S.-L.C.) from the American Heart Association.

References

[1] Cotran, R. S.; Gimbrone, M. A., Jr; Bevilacqua, M. P.; Mendrick, D. L.; Pober, J. S. Induction and detection of a human endothelial activation antigen in vivo. *J. Exp. Med.* **1986**, *164*(2), 661–666.

[2] Konstantopoulos, K.; Kukreti, S.; McIntire, L. V. Biomechanics of cell interactions in shear fields. *Adv. Drug. Deliv. Rev.* **1998**, *33*(1-2), 141–164.

[3] Yao, L.; Pan, J.; Setiadi, H.; Patel, K. D.; McEver, R. P. Interleukin 4 or oncostatin M induces a prolonged increase in P-selectin mRNA and protein in human endothelial cells. *J. Exp. Med.* **1996**, *184*(1), 81–92.

[4] Kansas, G. S. Selectins and their ligands: current concepts and controversies. *Blood* **1996**, *88*(9), 3259–3287.

[5] Somers, W. S.; Tang, J.; Shaw, G. D.; Camphausen, R. T. Insights into the molecular basis of leukocyte tethering and rolling revealed by structures of P- and E-selectin bound to SLe(X) and PSGL-1. *Cell* **2000**, *103*(3), 467–479.

[6] Patel, K. D.; Nollert, M. U.; McEver, R. P. P-selectin must extend a sufficient length from the plasma membrane to mediate rolling of neutrophils. *Journal of Cell Biology* **1995**, *131*(6), 1893–1902.

[7] Varki, A. Selectin ligands: will the real ones please stand up? *J. Clin. Invest.* **1997**, *100*(11), Suppl. S31–35.

[8] McEver, R. P.; Cummings, R. D. Perspectives series: cell adhesion in vascular biology. Role of PSGL-1 binding to selectins in leukocyte recruitment. *J. Clin. Invest.* **1997**, *100*(3), 485–491.

[9] Frenette, P. S.; Denis, C. V.; Weiss, L.; Jurk, K.; Subbarao, S.; Kehrel, B.; Hartwig, J. H.; Vestweber, D.; Wagner, D. D. P-Selectin glycoprotein ligand 1 (PSGL-1) is expressed on platelets and can mediate platelet-endothelial interactions in vivo. *J. Exp. Med.* **2000**, *191*(8), 1413–1422.

[10] Leppanen, A.; White, S. P.; Helin, J.; McEver, R. P.; Cummings, R. D. Binding of glycosulfopeptides to P-selectin requires stereospecific contributions of individual tyrosine sulfate and sugar residues. *Journal of Biological Chemistry* **2000**, *275*(50), 39569–39578.

[11] Rosen, S. D. Ligands for L-selectin: homing, inflammation, and beyond. *Annu. Rev. Immunol.* **2004**, *22*, 129–156.

[12] Hanley, W. D.; Wirtz, D.; Konstantopoulos, K. Distinct kinetic and mechanical properties govern selectin-leukocyte interactions. *J. Cell Sci.* **2004**, *117*(Pt 12), 2503–2511.

[13] Alon, R.; Feizi, T.; Yuen, C. T.; Fuhlbrigge, R. C.; Springer, T. A. Glycolipid ligands for selectins support leukocyte tethering and rolling under physiologic flow conditions. *J. Immunol.* **1995**, *154*(10), 5356–5366.

[14] Burdick, M. M.; Bochner, B. S.; Collins, B. E.; Schnaar, R. L.; Konstantopoulos, K. Glycolipids support E-selectin-specific strong cell tethering under flow. *Biochem. Biophys. Res. Commun.* **2001**, *284*(1), 42–49.

[15] Nimrichter, L.; Burdick, M. M.; Aoki, K.; Laroy, W.; Fierro, M. A.; Hudson, S. A.; Von Seggern, C. E.; Cotter, R. J.; Bochner, B. S.; Tiemeyer, M.; Konstantopoulos, K. R. L. S. E-selectin receptors on human leukocytes. *Blood* **2008**, *112*(9), 3744–3752.

[16] Hanley, W. D.; Burdick, M. M.; Konstantopoulos, K.; Sackstein, R. CD44 on LS174T colon carcinoma cells possesses E-selectin ligand activity. *Cancer Res.* **2005**, *65*(13), 5812–5817.

[17] Hanley, W. D.; Napier, S. L.; Burdick, M. M.; Schnaar, R. L.; Sackstein, R.; Konstantopoulos, K. Variant isoforms of CD44 are P- and L-selectin ligands on colon carcinoma cells. *FASEB J.* **2006**, *20*(2), 337–339.

[18] Napier, S. L.; Healy, Z. R.; Schnaar, R. L.; Konstantopoulos, K. Selectin ligand expression regulates the initial vascular interactions of colon carcinoma cells: The roles of CD44V and alternative sialofucosylated selectin ligands. *J. Biol. Chem.* **2007**, *282*(6), 3433–3441.

[19] Piper, J. W.; Swerlick, R. A.; Zhu, C. Determining force dependence of two-dimensional receptor–ligand binding affinity by centrifugation. *Biophys. J.* **1998**, *74*(1), 492–513.

[20] Evans, E.; Berk, D.; Leung, A. Detachment of Agglutinin-Bonded Red-Blood-Cells. 1. Forces to Rupture Molecular-Point Attachments. *Biophysical Journal* **1991**, *59*(4), 838–848.

[21] Evans, E.; Berk, D.; Leung, A. Detachment of agglutinin-bonded red blood cells. I. Forces to rupture molecular-point attachments. *Biophys. J.* **1991**, *59*(4), 838–848.

[22] Evans, E.; Ritchie, K.; Merkel, R. Sensitive force technique to probe molecular adhesion and structural linkages at biological interfaces. *Biophys. J.* **1995**, *68*(6), 2580–2587.

[23] Chesla, S. E.; Selvaraj, P.; Zhu, C. Measuring two-dimensional receptor–ligand binding kinetics by micropipette. *Biophys. J.* **1998**, *75*(3), 1553–1572.

[24] McQuarrie, D. A. Kinetics of Small Systems .1. *J. Chem. Phys.* **1963**, *38*(2), 433–436.

[25] McQuarrie, D. A.; Russell, M. E.; Jachimowicz, C. J. Kinetics of Small Systems 2. *J. Chem. Phys.* **1964**, *40*(10), 2914–2921.

[26] Cozens-Roberts, C.; Lauffenburger, D. A.; Quinn, J. A. Receptor-Mediated Cell Attachment and Detachment Kinetics .1. Probabilistic Model and Analysis. *Biophysical Journal* **1990**, *58*(4), 841–856.

[27] Cozens-Roberts, C.; Quinn, J. A.; Lauffenburger, D. A. Receptor-Mediated Cell Attachment and Detachment Kinetics 2. Experimental-Model Studies with the Radial-Flow Detachment Assay. *Biophysical Journal* **1990**, *58*(4), 857–872.

[28] Kaplanski, G.; Farnarier, C.; Tissot, O.; Pierres, A.; Benoliel, A. M.; Alessi, M. C.; Kaplanski, S.; Bongrand, P. Granulocyte-endothelium initial adhesion. Analysis of transient binding events mediated by E-selectin in a laminar shear flow. *Biophys. J.* **1993**, *64*(6), 1922–1933.

[29] Long, M. A.; Goldsmith, H. L.; Tees, D. F. J.; Zhu, C. Probabilistic modeling of shear-induced formation and breakage of doublets cross-linked by receptor–ligand bonds. *Biophysical Journal* **1999**, *76*(2), 1112–1128.

[30] Capo, C.; Garrouste, F.; Benoliel, A. M.; Bongrand, P.; Ryter, A.; Bell, G. I. Concanavalin-A-mediated thymocyte agglutination: a model for a quantitative study of cell adhesion. *J. Cell Sci.* **1982**, *56*, 21–48.

[31] Chesla, S. E.; Li, P.; Nagarajan, S.; Selvaraj, P.; Zhu, C. The membrane anchor influences ligand binding two-dimensional kinetic rates and three-dimensional affinity of FcgammaRIII (CD16). *J. Biol. Chem.* **2000**, *275*(14), 10235–10246.

[32] Williams, T. E.; Nagarajan, S.; Selvaraj, P.; Zhu, C. Concurrent and independent binding of Fcgamma receptors IIa and IIIb to surface-bound IgG. *Biophys. J.* **2000**, *79*(4), 1867–1875.

[33] Williams, T. E.; Selvaraj, P.; Zhu, C. Concurrent binding to multiple ligands: kinetic rates of CD16b for membrane-bound IgG1 and IgG2. *Biophys. J.* **2000**, *79*(4), 1858–1866.

[34] Zhu, C.; Bao, G.; Wang, N. Cell mechanics: mechanical response, cell adhesion, and molecular deformation. *Annu. Rev. Biomed. Eng.* **2000**, *2*, 189–226.

[35] Huang, J.; Chen, J.; Chesla, S. E.; Yago, T.; Mehta, P.; McEver, R. P.; Zhu, C.; Long, M. Quantifying the effects of molecular orientation and length on two-dimensional receptor–ligand binding kinetics. *J. Biol. Chem.* **2004**, *279*(43), 44915–44923.

[36] Wu, L.; Xiao, B.; Jia, X.; Zhang, Y.; Lu, S.; Chen, J.; Long, M. Impact of carrier stiffness and microtopology on two-dimensional kinetics of P-selectin and P-selectin glycoprotein ligand-1 (PSGL-1) interactions. *J. Biol. Chem.* **2007**, *282*(13), 9846–9854.

[37] Alon, R.; Chen, S.; Fuhlbrigge, R.; Puri, K. D.; Springer, T. A. The kinetics and shear threshold of transient and rolling interactions of L-selectin with its ligand on leukocytes. *Proc. Natl. Acad. Sci. U S A* **1998**, *95*(20), 11631–11636.

[38] Alon, R.; Chen, S.; Puri, K. D.; Finger, E. B.; Springer, T. A. The kinetics of L-selectin tethers and the mechanics of selectin-mediated rolling. *J. Cell. Biol.* **1997**, *138*(5), 1169–1180.

[39] Smith, M. J.; Berg, E. L.; Lawrence, M. B. A direct comparison of selectin-mediated transient, adhesive events using high temporal resolution. *Biophys. J.* **1999**, *77*(6), 3371–3383.

[40] Dobrowsky, T. M.; Panorchan, P.; Konstantopoulos, K.; Wirtz, D. Live-cell single-molecule force spectroscopy. Chapter 15. *Methods Cell Biol.* **2008**, *89*, 411–432.

[41] Evans, E.; Leung, A.; Hammer, D.; Simon, S. Chemically distinct transition states govern rapid dissociation of single L-selectin bonds under force. *Proc. Natl. Acad. Sci. U S A* **2001**, *98*(7), 3784–3789.

[42] Evans, E.; Leung, A.; Heinrich, V.; Zhu, C. Mechanical switching and coupling between two dissociation pathways in a P-selectin adhesion bond. *Proc. Natl. Acad. Sci. U S A* **2004**, *101*(31), 11281–11286.

[43] Evans, E. A.; Calderwood, D. A. Forces and bond dynamics in cell adhesion. *Science* **2007**, *316*(5828), 1148–1153.

[44] Hanley, W.; McCarty, O.; Jadhav, S.; Tseng, Y.; Wirtz, D.; Konstantopoulos, K. Single molecule characterization of P-selectin/ligand binding. *J. Biol. Chem.* **2003**, *278*(12), 10556–10561.

[45] Marshall, B. T.; Long, M.; Piper, J. W.; Yago, T.; McEver, R. P.; Zhu, C. Direct observation of catch bonds involving cell-adhesion molecules. *Nature* **2003**, *423*(6936), 190–193.

[46] Sarangapani, K. K.; Yago, T.; Klopocki, A. G.; Lawrence, M. B.; Fieger, C. B.; Rosen, S. D.; McEver, R. P.; Zhu, C. Low force decelerates L-selectin dissociation from P-selectin glycoprotein ligand-1 and endoglycan. *Journal of Biological Chemistry* **2004**, *279*(3), 2291–2298.

[47] Evans, E. Probing the relation between force–lifetime–and chemistry in single molecular bonds. *Annu. Rev. Biophys. Biomol. Struct.* **2001**, *30*, 105–128.

[48] Helenius, J.; Heisenberg, C. P.; Gaub, H. E.; Muller, D. J. Single-cell force spectroscopy. *J. Cell Sci.* **2008**, *121*(Pt 11), 1785–1791.

[49] Muller, D. J.; Dufrene, Y. F. Atomic force microscopy as a multifunctional molecular toolbox in nanobiotechnology. *Nat. Nanotechnol.* **2008**, *3*(5), 261–269.

[50] Muller, D. J.; Helenius, J.; Alsteens, D.; Dufrene, Y. F. Force probing surfaces of living cells to molecular resolution. *Nat. Chem. Biol.* **2009**, *5*(6), 383–390.

[51] Puchner, E. M.; Alexandrovich, A.; Kho, A. L.; Hensen, U.; Schafer, L. V.; Brandmeier, B.; Grater, F.; Grubmuller, H.; Gaub, H. E.; Gautel, M. Mechanoenzymatics of titin kinase. *P. Natl. Acad. Sci. USA* **2008**, *105*(36), 13385–13390.

[52] del Rio, A.; Perez-Jimenez, R.; Liu, R. C.; Roca-Cusachs, P.; Fernandez, J. M.; Sheetz, M. P. Stretching Single Talin Rod Molecules Activates Vinculin Binding. *Science* **2009**, *323*(5914), 638–641.

[53] Fritz, J.; Katopodis, A. G.; Kolbinger, F.; Anselmetti, D. Force-mediated kinetics of single P-selectin/ligand complexes observed by atomic force microscopy. *Proc. Natl. Acad. Sci. U S A* **1998**, *95*(21), 12283–12288.

[54] Zhang, X.; Wojcikiewicz, E.; Moy, V. T. Force spectroscopy of the leukocyte function-associated antigen-1/intercellular adhesion molecule-1 interaction. *Biophys. J.* **2002**, *83*(4), 2270–2279.

[55] Panorchan, P.; Thompson, M. S.; Davis, K. J.; Tseng, Y.; Konstantopoulos, K.; Wirtz, D. Single-molecule analysis of cadherin-mediated cell-cell adhesion. *Journal of Cell Science* **2006**, *119*(1), 66–74.

[56] Bershadsky, A.; Kozlov, M.; Geiger, B. Adhesion-mediated mechanosensitivity: a time to experiment, and a time to theorize. *Curr. Opin. Cell Biol.* **2006**, 18(5), 472–481.

[57] Benoit, M.; Gabriel, D.; Gerisch, G.; Gaub, H. E. Discrete interactions in cell adhesion measured by single-molecule force spectroscopy. *Nat. Cell Biol.* **2000**, *2*(6), 313–317.

[58] Zhang, X.; Craig, S. E.; Kirby, H.; Humphries, M. J.; Moy, V. T. Molecular basis for the dynamic strength of the integrin alpha4beta1/VCAM-1 interaction. *Biophys. J.* **2004**, *87*(5), 3470–3478.

[59] Wojcikiewicz, E. P.; Abdulreda, M. H.; Zhang, X.; Moy, V. T. Force spectroscopy of LFA-1 and its ligands, ICAM-1 and ICAM-2. *Biomacromolecules* **2006**, *7*(11), 3188–3195.

[60] Bell, G. I. Models for the specific adhesion of cells to cells. *Science* **1978**, *200*(4342), 618–627.

[61] Merkel, R.; Nassoy, P.; Leung, A.; Ritchie, K.; Evans, E. Energy landscapes of receptor–ligand bonds explored with dynamic force spectroscopy. *Nature* **1999**, *397*(6714), 50–53.

[62] Evans, E.; Ritchie, K. Dynamic strength of molecular adhesion bonds. *Biophys. J.* **1997**, *72*(4), 1541–1555.

[63] Tees, D. F.; Waugh, R. E.; Hammer, D. A. A microcantilever device to assess the effect of force on the lifetime of selectin-carbohydrate bonds. *Biophys. J.* **2001**, *80*(2), 668–682.

[64] Alon, R.; Hammer, D. A.; Springer, T. A. Lifetime of the P-Selectin-Carbohydrate Bond and Its Response to Tensile Force in Hydrodynamic Flow. *Nature* **1995**, *374*(6522), 539–542.

[65] Dembo, M.; Torney, D. C.; Saxman, K.; Hammer, D. The Reaction-Limited Kinetics of Membrane-to-Surface Adhesion and Detachment. *P. Roy. Soc. Lond. B. Bio.* **1988**, *234*(1274), 55–83.

[66] Yago, T.; Wu, J.; Wey, C. D.; Klopocki, A. G.; Zhu, C.; McEver, R. P. Catch bonds govern adhesion through L-selectin at threshold shear. *J. Cell Biol.* **2004**, *166*(6), 913–923.

[67] Finger, E. B.; Puri, K. D.; Alon, R.; Lawrence, M. B.; von Andrian, U. H.; Springer, T. A. Adhesion through L-selectin requires a threshold hydrodynamic shear. *Nature* **1996**, *379*(6562), 266–269.

[68] Lawrence, M. B.; Kansas, G. S.; Kunkel, E. J.; Ley, K. Threshold levels of fluid shear promote leukocyte adhesion through selectins (CD62L,P,E). *J. Cell Biol.* **1997**, *136*(3), 717–727.

[69] Yago, T.; Lou, J.; Wu, T.; Yang, J.; Miner, J. J.; Coburn, L.; Lopez, J. A.; Cruz, M. A.; Dong, J. F.; McIntire, L. V.; McEver, R. P.; Zhu, C. Platelet glycoprotein Ibalpha forms catch bonds with human WT vWF but not with type 2B von Willebrand disease vWF. *J. Clin. Invest.* **2008**, *118*(9), 3195–3207.

[70] Thomas, W. E.; Trintchina, E.; Forero, M.; Vogel, V.; Sokurenko, E. V. Bacterial adhesion to target cells enhanced by shear force. *Cell* **2002**, *109*(7), 913–923.

[71] Thomas, W. E.; Vogel, V.; Sokurenko, E. Biophysics of catch bonds. *Annu. Rev. Biophys.* **2008**, *37*, 399–416.

[72] Pereverzev, Y. V.; Prezhdo, O. V.; Forero, M.; Sokurenko, E. V.; Thomas, W. E. The two-pathway model for the catch-slip transition in biological adhesion. *Biophysical Journal* **2005**, *89*(3), 1446–1454.

[73] Konstantopoulos, K.; Hanley, W. D.; Wirtz, D. receptor–ligand binding: 'catch' bonds finally caught. *Curr. Biol.* **2003**, *13*(15), R611–613.

[74] Lou, J.; Yago, T.; Klopocki, A. G.; Mehta, P.; Chen, W.; Zarnitsyna, V. I.; Bovin, N. V.; Zhu, C.; McEver, R. P. Flow-enhanced adhesion regulated by a selectin interdomain hinge. *J. Cell Biol.* **2006**, *174*(7), 1107–1117.

[75] Lou, J. Z.; Zhu, C. A structure-based sliding-rebinding mechanism for catch bonds. *Biophysical Journal* **2007**, *92*(5), 1471–1485.

[76] Caputo, K. E.; Lee, D.; King, M. R.; Hammer, D. A. Adhesive dynamics simulations of the shear threshold effect for leukocytes. *Biophys. J.* **2007**, *92*(3), 787–797.

[77] Pawar, P.; Jadhav, S.; Eggleton, C. D.; Konstantopoulos, K. Roles of cell and microvillus deformation and receptor–ligand binding kinetics in cell rolling. *Am. J. Physiol. Heart Circ. Physiol.* **2008**, *295*(4), H1439–1450.

[78] Jadhav, S.; Konstantopoulos, K. Fluid shear- and time-dependent modulation of molecular interactions between polymorphonuclear leukocytes and colon carcinomas. *Am. J. Physiology Cell Physiology* **2002**, *283*(4), C1133–1143.

[79] Taylor, A. D.; Neelamegham, S.; Hellums, J. D.; Smith, C. W.; Simon, S. I. Molecular dynamics of the transition from L-selectin- to beta 2-integrin-dependent neutrophil adhesion under defined hydrodynamic shear. *Biophys. J.* **1996**, *71*(6), 3488–3500.

[80] Zhu, C.; Lou, J.; McEver, R. P. Catch bonds: physical models, structural bases, biological function and rheological relevance. *Biorheology* **2005**, *42*(6), 443–462.

[81] Jadhav, S.; Eggleton, C. D.; Konstantopoulos, K. Mathematical modeling of cell adhesion in shear flow: Application to targeted drug delivery in inflammation and cancer metastasis. *Curr. Pharm. Design.* **2007**, *13*(15), 1511–1526.

[82] Konstantopoulos, K.; Thomas, S. N. Cancer cells in transit: the vascular interactions of tumor cells. *Annu. Rev. Biomed. Eng.* **2009**, *11*, 177–202.

[83] McCarty, O. J.; Mousa, S. A.; Bray, P. F.; Konstantopoulos, K. Immobilized platelets support human colon carcinoma cell tethering, rolling, and firm adhesion under dynamic flow conditions. *Blood* **2000**, *96*(5), 1789–1797.

[84] Mannori, G.; Santoro, D.; Carter, L.; Corless, C.; Nelson, R. M.; Bevilacqua, M. P. Inhibition of colon carcinoma cell lung colony formation by a soluble form of E-selectin. *Am. J. Pathol.* **1997**, *151*(1), 233–243.

[85] Lawrence, M. B.; Springer, T. A. Leukocytes roll on a selectin at physiologic flow rates: distinction from and prerequisite for adhesion through integrins. *Cell* **1991**, *65*(5), 859–873.

[86] Chang, K. C.; Tees, D. F.; Hammer, D. A. The state diagram for cell adhesion under flow: leukocyte rolling and firm adhesion. *Proc. Natl. Acad. Sci. U S A* **2000**, *97*(21), 11262–11267.

[87] Krasik, E. F.; Hammer, D. A. A semianalytic model of leukocyte rolling. *Biophys. J.* **2004**, *87*(5), 2919–2930.

[88] Goldman, A. J.; Cox, R. G.; Brenner, H. Slow viscous motion of a sphere parallel to a plane wall 2. couette flow. *Chem. Eng. Sci.* **1967**, *22*(4), 653–660.

[89] Chen, S.; Alon, R.; Fuhlbrigge, R. C.; Springer, T. A. Rolling and transient tethering of leukocytes on antibodies reveal specializations of selectins. *Proc. Natl. Acad. Sci. U S A* **1997**, *94*(7), 3172–3177.

[90] Shao, J. Y.; Ting-Beall, H. P.; Hochmuth, R. M. Static and dynamic lengths of neutrophil microvilli. *Proc. Natl. Acad. Sci. U S A* **1998**, *95*(12), 6797–6802.

[91] Hammer, D. A.; Apte, S. M. Simulation of cell rolling and adhesion on surfaces in shear flow: general results and analysis of selectin-mediated neutrophil adhesion. *Biophys. J.* **1992**, *63*(1), 35–57.

[92] Puri, K. D.; Finger, E. B.; Springer, T. A. The faster kinetics of L-selectin than of E-selectin and P-selectin rolling at comparable binding strength. *Journal of Immunology* **1997**, *158*(1), 405–413.

[93] Tozeren, A.; Ley, K. How do selectins mediate leukocyte rolling in venules? *Biophys. J.* **1992**, *63*(3), 700–709.

[94] Cichocki, B.; Jones, R. B. Image representation of a spherical particle near a hard wall. *Physica. A.* **1998**, *258*(3-4), 273–302.

[95] Perkins, G. S.; Jones, R. B. Hydrodynamic Interaction of a Spherical-Particle with a Planar Boundary .2. Hard-Wall. *Physica. A.* **1992**, *189*(3-4), 447–477.

[96] Chang, K. C.; Hammer, D. A. The forward rate of binding of surface-tethered reactants: effect of relative motion between two surfaces. *Biophys. J.* **1999**, *76*(3), 1280–1292.

[97] Zhu, C.; Yago, T.; Lou, J.; Zarnitsyna, V. I.; McEver, R. P. Mechanisms for flow-enhanced cell adhesion. *Ann. Biomed. Eng.* **2008**, *36*(4), 604–621.

[98] Orsello, C. E.; Lauffenburger, D. A.; Hammer, D. A. Molecular properties in cell adhesion: a physical and engineering perspective. *Trends Biotechnol.* **2001**, *19*(8), 310–316.

[99] Ramachandran, V.; Nollert, M. U.; Qiu, H. Y.; Liu, W. J.; Cummings, R. D.; Zhu, C.; McEver, R. P. Tyrosine replacement in P-selectin glycoprotein ligand-1 affects distinct kinetic and mechanical properties of bonds with P- and L-selectin. *P. Natl. Acad. Sci. U S A* **1999**, *96*(24), 13771–13776.

[100] Hochmuth, R. M.; Ting-Beall, H. P.; Beaty, B. B.; Needham, D.; Tran-Son-Tay, R. Viscosity of passive human neutrophils undergoing small deformations. *Biophys. J.* **1993**, *64*(5), 1596–1601.

[101] Hochmuth, R. M. Micropipette aspiration of living cells. *J. Biomech.* **2000**, *33*(1), 15–22.

[102] Drury, J. L.; Dembo, M. Aspiration of human neutrophils: effects of shear thinning and cortical dissipation. *Biophys. J.* **2001**, *81*(6), 3166–3177.

[103] Drury, J. L.; Dembo, M. Hydrodynamics of micropipette aspiration. *Biophys. J.* **1999**, *76*(1 Pt 1), 110–128.

[104] Herant, M.; Heinrich, V.; Dembo, M. Mechanics of neutrophil phagocytosis: behavior of the cortical tension. *J. Cell Sci.* **2005**, *118*(Pt 9), 1789–1797.

[105] Tsai, M. A.; Frank, R. S.; Waugh, R. E. Passive mechanical behavior of human neutrophils: power-law fluid. *Biophys. J.* **1993**, *65*(5), 2078–2088.

[106] Herant, M.; Marganski, W. A.; Dembo, M. The mechanics of neutrophils: synthetic modeling of three experiments. *Biophys. J.* **2003**, *84*(5), 3389–3413.

[107] Dong, C.; Cao, J.; Struble, E. J.; Lipowsky, H. H. Mechanics of leukocyte deformation and adhesion to endothelium in shear flow. *Ann. Biomed. Eng.* **1999**, *27*(3), 298–312.

[108] Dong, C.; Lei, X. X. Biomechanics of cell rolling: shear flow, cell-surface adhesion, and cell deformability. *J. Biomech.* **2000**, *33*(1), 35–43.

[109] N'Dri, N. A.; Shyy, W.; Tran-Son-Tay, R. Computational modeling of cell adhesion and movement using a continuum-kinetics approach. *Biophys. J.* **2003**, *85*(4), 2273–2286.

[110] Schmidtke, D. W.; Diamond, S. L. Direct observation of membrane tethers formed during neutrophil attachment to platelets or P-selectin under physiological flow. *J. Cell Biol.* **2000**, *149*(3), 719–730.

[111] Marella, S. V.; Udaykumar, H. S. Computational analysis of the deformability of leukocytes modeled with viscous and elastic structural components. *Phys. Fluids* **2004**, *16*(2), 244–264.

[112] Khismatullin, D. B.; Truskey, G. A. A 3D numerical study of the effect of channel height on leukocyte deformation and adhesion in parallel-plate flow chambers. *Microvasc. Res.* **2004**, *68*(3), 188–202.

[113] Khismatullin, D. B.; Truskey, G. A Three-dimensional numerical simulation of receptor-mediated leukocyte adhesion to surfaces: Effects of cell deformability and viscoelasticity. *Phys. Fluids* **2005**, *17*(3), 031505.

[114] Jadhav, S.; Eggleton, C. D.; Konstantopoulos, K. A 3-D computational model predicts that cell deformation affects selectin-mediated leukocyte rolling. *Biophys. J.* **2005**, *88*(1), 96–104.

[115] Peskin, C. S.; McQueen, D. M. A 3-Dimensional computational method for blood-flow in the heart 1. immersed elastic fibers in a viscous incompressible fluid. *J. Comput. Phys.* **1989**, *81*(2), 372–405.

[116] Dembo, M.; Torney, D. C.; Saxman, K.; Hammer, D. The reaction-limited kinetics of membrane-to-surface adhesion and detachment. *Proc. R. Soc. Lond. B. Biol. Sci.* **1988**, *234*(1274), 55–83.

[117] Park, E. Y.; Smith, M. J.; Stropp, E. S.; Snapp, K. R.; DiVietro, J. A.; Walker, W. F.; Schmidtke, D. W.; Diamond, S. L.; Lawrence, M. B. Comparison of PSGL-1 microbead and neutrophil rolling: microvillus elongation stabilizes P-selectin bond clusters. *Biophys. J.* **2002**, *82*(4), 1835–1847.

[118] Yago, T.; Leppanen, A.; Qiu, H.; Marcus, W. D.; Nollert, M. U.; Zhu, C.; Cummings, R. D.; McEver, R. P. Distinct molecular and cellular contributions to stabilizing selectin-mediated rolling under flow. *J. Cell Biol.* **2002**, *158*(4), 787–799.

[119] Nicholson, M. W.; Barclay, A. N.; Singer, M. S.; Rosen, S. D.; van der Merwe, P. A. Affinity and kinetic analysis of L-selectin (CD62L) binding to glycosylation-dependent cell-adhesion molecule-1. *J. Biol. Chem.* **1998**, *273*, 763–770.

[120] Poppe, L.; Brown, G. S.; Philo, J. S.; Nikrad, P. V.; Shah. Conformation of sLe(x) tetrasaccharide, free in solution and bound to E-, P-, and L-selectin. *J. Am. Chem. Soc.* **1997**, *119*, 1727–1736.

[121] Fay, F. S. Isometric contractile properties of single isolated smooth muscle cells. *Nature* **1977**, *265*, 553–556.

[122] Lee, G. U.; Chrisey, L. A.; Colton, R. J. Direct measurement of the forces between complementary strands of DNA. *Science* **1994**, *266*, 771–773.

[123] Lee, G. U.; Kidwell, D. A.; Colton, R. J. Sensing Discrete Streptavidin Biotin Interactions with Atomic-Force Microscopy. *Langmuir* **1994**, *10*, 354–357.

[124] Rief, M.; Gautel, M.; Oesterhelt, F.; Fernandez, J. M.; Gaub, H. E. Reversible unfolding of individual titin immunoglobulin domains by AFM. *Science* **1997**, *276*, 1109–1112.

[125] Hinterdorfer, P.; Dufrene, Y. F. Detection and localization of single molecular recognition events using atomic force microscopy. *Nat. Methods* **2006**, *3*, 347–355.

[126] Piazzesi, G.; Reconditi, M.; Linari, M.; Lucii, L.; Bianco, P.; Brunello, E.; Decostre, V.; Stewart, A.; Gore, D. B.; Irving, T. C.; Irving, M.; Lombardi, V. Skeletal muscle performance determined by modulation of number of myosin motors rather than motor force or stroke size. *Cell* **2007**, *131*, 784–795.